

1 **Manuscript # esurf-2020-37**

2 Answers to review comments

3 (Please note that the annotated manuscript file is attached separately)

4 Dear editor and reviewers,

5 First of all, I would like to thank all of you for such an in-depth review for our
6 manuscript. We really benefitted from your comments and suggestions. On behalf of the authors,
7 I am happy to tell you that we have made significant changes in the manuscript according to your
8 comments; especially we have looked more in detail in the geological background and discussion
9 section. This has increased the length of the manuscript by a bit, but I ensure that all your queries
10 are hopefully taken care of.

11 A few key changes-

- 12 a. Title has been revised.
- 13 b. Abstract has been revised and reduced in length.
- 14 c. End of introduction has been modified.
- 15 d. Geological background section: debate on structural setting of the Kishtwar Window
16 elaborated.
- 17 e. Methods: Luminescence sample process protocol is now moved to the appendix.
- 18 f. Results: Couple more OSL data included.
- 19 g. Discussion is revised to offer an open-ended view on the debate between duplex-growth
20 vs. active out-of-sequence faulting in the interior of the Kashmir Himalaya.
- 21 h. Conclusions revised accordingly.

22 Thank you again for considering our work.

23 On behalf of the authors

24 Saptarshi Dey

25

26

27

28 **Comments to reviewer #1**

29 1. General query regarding citations and figure references

30 Revised and rechecked twice.

31 2. Syntax errors and nomenclature issues.

32 Revised.

33 3. The geomorphic data still seem to be not fully consistent. Let us look, e.g., at the channel
34 slope and the steepness index k_{sn} in Fig. 6. They are related to each other by the factor
35 $A^{0.9}$ where A is the catchment size which increases downstream, i.e., from the right to
36 the left. Let us start from the right-hand edge where the slope increases while k_{sn}
37 immediately decreases to the left. Or look how much the large double peak at $x = 10$ km
38 is higher than the k_{sn} values at $x < 10$ km, and how much lower the relative difference in
39 slope is. This is in principle impossible. I am quite sure that this is not a fundamental
40 problem, maybe even only inconsistent smoothing of the data. I think it can be fixed
41 easily, but such things just do not make it easier to trust that everything is technically
42 sound -- although the most importing parts are probably.

43 Agreed and revised. You are right that there is some issue with smoothing. Probably the
44 preprocessing of the DEM data has some issues. Now we have used a 10 point smoothing
45 window throughout the entire stretch.

46

47 **Comments to reviewer #2**

48

49 1. Throughout the paper the authors are unclear or ambiguous how they characterize and
50 interpret patterns associated with “faulting”, “growth”, or “active surface faulting” across
51 the Kishtwar Window. For instance their cross section and map figures clearly indicate
52 their interpretation of an out-of-sequence surface breaking fault, however, in the text their
53 interpretation is unclear going back and forth between implying active faulting on MHT
54 crustal ramps (no surface faulting), to active duplex growth, to active out-of-sequence
55 deformation (surface faulting) that links to a crustal ramps. The authors need to clarify

56 and revise many of the structural terms and interpretations being used in the text to
57 streamline their interpretations.

58 Text has been revised. Now, we invite for an open interpretation of our results. We show
59 that our results can be explained by both duplex-growth model aided by differential uplift
60 over mid-crustal ramps or by active out-of-sequence faulting across the window.
61 Although our field observation questions the brittle-deforming duplex model, we neither
62 have any first-hand evidence for regional out-of-sequence faulting too.

63 2. The authors need to provide more justification in their interpretation that morphometric
64 indices provide evidence for or against active out-of-sequence faulting. In many places,
65 the authors jump to their preferred model but failed to recognize that these morphometric
66 indices or other structural data are non-unique! In other words, the authors do not provide
67 enough justification why or why not the pattern observed can be attributed to a specific
68 deformation pattern. The authors have a tendency to have model-driven interpretations
69 and do not justify why other structural models or non-tectonic controls are not
70 permissible. For instance, many of the arguments used by the authors as “evidence” of an
71 active out-of-sequence fault within the KW are not justified and highly speculative. Many
72 of the observation described by the authors can be equally or more easily explained of the
73 presence of an exhumed duplex floor thrust, and all of the knickpoints pattern are
74 controlled by translation across MHT ramp which require no surface faulting.

75 Revised in order to keep the interpretation open.

76 3. I believe there would be strong benefits in this paper to recognize that this an open-ended
77 interpretation (active out-of-sequence thrusting versus translation across MHT ramp). A
78 more constructive approach would be to offer two possible viable structural interpretation
79 of the cross section diagrams (out-of-sequence thrust versus and exhumed duplex floor
80 thrust with active deeper ramp along the MHT), and let the reader see how each models
81 can explain some of the observations.

82 Agreed and revised accordingly. Please refer to the end of discussion section (line #655-
83 696).

84 4. Interpretation of duplex or cross section needs revision. There are several keys issues
85 with the cross section listed below:

86

87 5. The figure shows an out-of-sequence thrust in the KW core that projects to cut roof
88 thrust. Because the author interprets as an out-of-sequence thrust, it implies it does not
89 join the roof thrust as duplex. Hence this is not consistent with the discussion in the text
90 that there is active/ongoing duplex growth. The diagram imply growth within KW occurs
91 via out-of-sequence thrusting (ramp #1), and translation of above MHT ramp (ramp #2).
92 There is no active/ongoing duplex kinematics as shown in the diagram.

93
94 Cross-section is revised in Fig.8d. We compare between ‘duplex-growth by slip on MHT’
95 model vs. ‘active out-of-sequence faulting’ models in Fig.8d. Both the models can
96 explain the observed morphometric variations.

97 6. This cross section does not appear to be restorable. Even If one would attempt to retro-
98 deform this cross section, it would show no duplex nor significant crustal thickening, but
99 instead a single nappe in the LHS that has been faulted by an out-of-sequence fault.

100 Our field observation tells that the Chail nappe exposed in the KW is internally buckle-
101 folded, pervasive folding and flexure has resulted into crustal thickening (please refer to
102 our field photos in Fig.2). This is supported by Fuchs (1975), Frank et al., (1995).

103 7. This cross section has major implications at odds with constraints from regional
104 shortening absorbed in the Kashmir Himalaya orogenic wedge. Available long-term
105 kinematics from low-temperature thermochron, Pleistocene-Holocene shortening rates,
106 and geodetic shortening rates across the Kashmir Sub-Himalaya imply that no significant
107 surface faulting within the KW or High Himalaya is needed to account for the total
108 budget of plate convergence absorbed in the Kashmir Himalaya.

109 Agreed. We see that over Quaternary and geodetic timescales, the total Himalayan
110 shortening is steady 13-15 mm/yr. Published shortening rates accommodated in Sub-
111 Himalaya over millennial timescales also hint similar amount of shortening rates. That
112 leaves no shortening to be accommodated beyond the MBT. But, this has a major
113 assumption that the total shortening rate since late Pleistocene is equal to other
114 timescales. This assumption has been questioned by the work of Vassallo et al., (2015).
115 In line with this, we do not pinpoint that ‘it has to be an out-of-sequence faulting in the
116 KW’, but ‘it could be an out-of-sequence faulting in the KW’.

117 8. d. The cross-section diagram is not consistent with duplex kinematics. Instead this pattern
118 is more aligned with antiformal dome with flexural flow within the structure (~local
119 crustal extrusion model).

120 The cross-section diagram has now been removed and revised. However, we like to
121 comment that the cross-section is a rough representation of field data and our field
122 observation goes against the existence of multiple nappes forming the duplex. In lieu of
123 that, we find tightly-folded Chail nappe in the window. Our observation is close to what
124 is proposed by Fuchs (1975) and Frank et al., (1995). In revision, we added the
125 comparison of two models – duplex-growth model (Gavillot et al., 2018) and out-of-
126 sequence model (Fig.8d). This keeps the manuscript open for the readers to decide which
127 one they favor.

128 9. Calculations and analyses of the shortening rates need substantive improvements. The
129 author makes incorrect assumptions that incision rate deduced west of KT and KW can
130 be translated to a shortening rate on the MCR1 fault ramp within the KW. For instance, if
131 looking at Fig. 8b, slip on the MCR-2 would not be translated with the same geometry to
132 the surface, as the underlying ramp-flat geometry would predict very little rock uplift
133 translated to the surface. I would recommend the author deletes text on the shortening
134 rate, because there is no data of incision rates in the upper plate of the inferred out-of-
135 sequence thrust to justify a calculation of shortening rate, and it is actually not relevant to
136 the main points of the paper. This section appears out of place for this paper.

137 We have deleted the discussion on shortening rates.

138 10. Much of the text and analyses on the OSL ages appear rushed and needs revision. Details
139 of OSL lab methodology ought to be placed in the supplement.

140 OSL methodology has been revised (line #337-356). Texts are added in justification of
141 luminescence ages. Additional information regarding OSL measurements given in
142 Supplementary figure B5.

143 11. There are still many unclear sentences that need revision. At times, there are also odd
144 choices of words and excessive use of unnecessary adjectives.

145 Sentences and ‘odd’ words have been revised thoroughly.

146 12. In Fig.6 and 7, knickpoint D1 and L2 not visible.

147 This is due to the scale of the graphic. The knickpoints are smaller (dz value: ~30m)
148 while the vertical scale is ~1cm = 500m/1000m and horizontal scale is 1cm = 20 km.
149 However, if you take a look in IFg.7d, you will observe slight increase in parameter
150 value. Said so, L2 is far downstream from our area of interest.

151

152 ** All the comments found in the annotated referee report is answered or addressed in the
153 revised version.

154 |

155 ~~Structural variations in basal decollement, internal deformation of the Lesser Himalayan~~
156 ~~Duplex and rapid fluvial incision modulate landscape morphology in NW Himalayan~~
157 ~~interiors~~Implications of the ongoing rock uplift in the NW Himalayan interiors

158 Saptarshi Dey¹, Rasmus Thiede², Arindam Biswas³, Naveen Chauhan⁴, Pritha Chakravarti¹, and
159 Vikrant Jain¹

160 ¹*Earth Science Discipline, IIT Gandhinagar, Gandhinagar-382355, India.*

161 ²*Institute of Geosciences, Christian Albrechts University of Kiel, Kiel-24118, Germany.*

162 ³*Department of Applied Geology, IIT-ISM Dhanbad, Jharkhand-826004, India.*

163 ⁴*Atomic Molecular and Optical physics Division, Physical Research Laboratory, Ahmedabad.*

164 Corresponding author

165 Saptarshi Dey

166 saptarshi.dey@iitgn.ac.in

167

168 **Abstract**

169 The Lesser Himalayan rocks exposed in the Kishtwar Window (KW) of the Kashmir
170 Himalaya exhibits rapid rock uplift and exhumation (~3 mm/yr) at least since the Late Miocene.
171 However, it has remained unclear if it is still actively-deforming. Here, we combine new field
172 observations, morphometric and structural analyses with dating of geomorphic markers to
173 discuss the spatial pattern of deformation across the window. We found two steep stream
174 segments, one at the core and the other along the western margin of the KW, which may possibly
175 be linked to crustal ramps on the MHT. Longitudinal fluvial profiles document gradients changes

176 across the entire length of the window, and high gradient changes in the core of the window.
177 High bedrock incision rates (> 3 mm/yr) are deduced from dated strath terraces along deeply-
178 incised Chenab River valley lying above the potential ramp along the western margin of the KW.
179 In contrast, farther downstream on the hanging wall of the MCT, fluvial bedrock incision rates
180 are lower (< 0.8 mm/yr). Bedrock incision rates largely correlate with previously-published
181 thermochronologic data. The obtained results can be partially explained by existence of multiple
182 crustal ramps which could result into differential uplift due to translation on the basal
183 decollement. Or, similar rock uplift can also be caused by out-of-sequence faulting at the core
184 and along the western margin of the window. In summary, our study highlights a structural and
185 tectonic control on landscape evolution over millennial timescales.

186 **Keywords**

187 Steepness index; knickzone, rock strength; bedrock incision; Main Himalayan Thrust.

188

189 **1. Introduction**

190

191 Protracted convergence between the Indian and the Eurasian plate resulted into the
192 growth and evolution of the Himalayan orogen and temporal in-sequence formation of the
193 Southern Tibetan Detachment System (STDS), the Main Central Thrust (MCT), the Main
194 Boundary Thrust (MBT) and the ~~Main Himalayan~~ Frontal Thrust (~~MFT~~HFT) towards the south
195 (e.g., Yin and Harrison, 2000; DiPietro and Pogue, 2004). HFT defines the southern termination
196 of the Himalayan orogenic wedge and separates the orogen from the undeformed foreland basin
197 known as the Indo-Gangetic Plains. Seismic reflection profiles reveal that all these fault-zones

198 emerge from a low-angle basal decollement, the Main Himalayan Thrust (MHT) forming the
199 base of the Himalayan orogenic wedge (e.g., Ni and Barazangi, 1984; Nabelek et al., 2009;
200 Avouac et al., 2016), established in the late Miocene (Vannay et al., 2004). Existence of MHT
201 has further been elaborated in Himalayan cross-sections (e.g., Powers et al., 1998; Decelles et al.,
202 2001; Webb et al., 2011; Gavillot et al., 2018).

203 Lave and Avouac (2000) studied the late Pleistocene-Holocene shortening history of the
204 Central Nepal Himalaya where they showed the Holocene shortening is accommodated only
205 across the HFT. Majority of scientists have However, a large body of literature in the eastern,
206 central and western Himalaya favored that majority of the late Pleistocene-Holocene shortening
207 of the Himalaya is mostly accommodated within the southern margin of the wedge, rather
208 partitioned throughout the Sub-Himalayan domain (morphotectonic segment in between the
209 MBT and the MFT) and not solely accommodated by the HFT (e.g., Wesnousky et al., 1999;
210 Lave and Avouac, 2000; Burgess et al., 2012; Thakur et al., 2014; Mukherjee, 2015; Vassalo et
211 al., 2015; Dey et al., 2016; Dey et al., 2018). The statement above implies that the northerly
212 thrusts, i.e., the MBT and the brittle faults exposed in the vicinity of the southern margin of the
213 Higher Himalaya, are considered inactive over millennial timescales. However, in recent years,
214 several studies which focused on the low-Temperature thermochronologic data and thermal
215 modeling of the interiors of the NW Himalaya have raised questions on the statement above. The
216 recent studies suggested that ~~10-15%~~ 1-3 mm/yr out of the total Quaternary shortening has been
217 accommodated in the north of the MBT as out-of-sequence deformation (Thiede et al., 2004;
218 Deeken et al., 2011; Thiede et al., 2017) or in form of growth of the Lesser Himalayan Duplex
219 (Gavillot et al., 2018) (Supplementary Fig. B1). ~~Overall~~ For faults within the hinterland of the
220 Central Himalaya, the out-of-sequence deformation ~~of the Himalayan wedge~~ has been explained

221 by two end-member models. One of them favored the reactivation of the MCT (Wobus et al.,
222 2003), while the other tried to explain all changes along the southern margin of the Higher
223 Himalaya driven by enhanced rock uplift over a major ramp on the MHT (Bollinger et al., 2006;
224 Herman et al., 2010; Robert et al., 2009). Landscape evolution models, structural analysis and
225 thermochronologic data from the interior of the Himalaya favor that the Lesser Himalaya has
226 formed a duplex at the base of the southern Himalayan front by sustained internal deformation
227 since late Miocene (Decelles et al., 2001; Mitra et al., 2010; Robinson and Martin, 2014; [Gavillot
228 et al., 2016](#)). The growth of the duplex resulted into the uplift of the Higher Himalaya forming
229 the major orographic barrier of the orogen. The Kishtwar Window (KW) in the NW Himalaya
230 represents the northwestern termination of the Lesser Himalayan Duplex (LHD). While most of
231 the published cross-sections of the Himalayan orogen today recognize the duplex [structures
232 within the Lesser Himalaya](#) (Webb et al., 2011; Mitra et al., 2010; DeCelles et al., 2001; [Gavillot
233 et al., 2018](#)), ~~usually very~~ little or no data are available on how the deformation is spatially as
234 well as temporally distributed and most importantly, whether [a](#) duplex is active over millennial
235 timescales.

236 The ~~pioneering~~ low-temperature thermochron study by Kumar et al., (1995) portrayed the
237 first orogen-perpendicular sampling traverse extending from the Kishtwar tectonic Window over
238 the Zaskar Range. More recent studies link the evolution of the KW to the growth of ~~a~~ [the](#)
239 Lesser Himalayan Duplex structure (Gavillot et al., 2018), surrounded by the Miocene MCT
240 shear zone along the base of the High Himalayan Crystalline, locally named as the Kishtwar
241 Thrust (KT) [\(Ul Haq et al., 2019\)](#). Thermochronological constraints suggest higher rates of
242 exhumation within the window (3.2-3.6 mm/yr) [with respect to the surroundings \(~0.2 mm/yr\)](#)
243 (Gavillot et al., 2018), corroborating well with similar thermochron-based findings from the of

244 the Kullu-Rampur window along the Beas (Stübner et al., (2018) and Sutlej valley (Jain et al.,
245 2000; Vannay et al., 2004; Thiede et al., 2004) over the Quaternary timescale. No evidence exists
246 whether the hinterland of the Kashmir Himalaya is tectonically-active over intermediate
247 timescales. Therefore, to understand the 10^3 - 10^4 -year timescale neotectonic evolution, ~~either we~~
248 ~~have to~~ combined ~~have~~ geological field evidences, chronologically-constrained geomorphic
249 markers ~~or at least have a rigorous and morphometric analysis~~ of potential study areas, such as
250 the KW. The detailed structural information of the window and the surroundings, previously-
251 published thermochron data, accessibility, well-preserved sediment archive, and recognizable
252 geomorphic markers across the Kishtwar Window makes it a potent location for our study.

253 In this study, we ~~will~~ focus on ~~few~~ the following long-standing questions on Himalayan
254 neotectonic evolution, which are-

255 1. ~~What is the spatial extent of neotectonic deformation, if any, in the interiors of the~~
256 ~~Himalaya~~ Is there any ongoing neotectonic deformation in the interiors of the Kashmir Himalaya?

257 ~~32. How reliably can we infer about sub-surface structural variations of the orogenic~~
258 ~~wedge by analyzing the terrain morphology~~ Can we determine sub-surface structural variations
259 and existence of surface-breaking faults by analyzing terrain morphology?

260 ~~43. Can we obtain new constraints on deformation over geomorphic timescales? Do~~
261 ~~millennial-scale fluvial incision rates support long-term exhumation rates?~~

262 To address these questions, we adopted a combination of methods such as morphometric
263 analysis using high-resolution digital elevation models, field observation on rock type, structural
264 variations as well as rock strength data ~~collection~~ and, analysis of satellite images to assess the
265 spatial distribution of the late Quaternary deformation of the KW and surroundings (Fig.1). ~~Our~~

266 ~~aim was to test if the landscape morphology can be explained by changes in the basal~~
267 ~~decollement and associated active structures, likewise it has been done in the neighboring sectors~~
268 ~~of the Himalaya~~We aimed to evaluate the role of active tectonics and geometric variations in the
269 basal decollement in shaping the topography (Fig.1). We used basinwide steepness indices and
270 specific stream power as a proxy of fluvial incision. And, lastly but most importantly, we ~~are~~
271 ~~able to constrain~~calculated the fluvial bedrock incision rates by using depositional ages of
272 aggraded sediments along Chenab River. ~~Our morphometric results document~~In this study, we
273 show that the regional distribution of ~~faulting topographic growth~~ is concentrated in the core of
274 the window and along the western margin of the window. ~~and indicated that active faulting~~
275 ~~within the Lesser Himalayan Duplex is controlling the ongoing deformation in the Himalayan~~
276 ~~interior and driving the uplift of Higher Himalaya in its hanging wall~~. Our new estimates on the
277 bedrock incision rate agree with Quaternary exhumation rates from the KW, which could mean
278 consistent active growth of the Kishtwar Window over million-year to millennial timescales.
279 Although the observed topographic and morphometric pattern indicate a structural/tectonic
280 control on topographic evolution, with the available data we are not able to resolve whether it is
281 caused by passive translation on the MHT or by active surface-breaking faulting within the
282 duplex.

283

284 2. Geological background

285 Regionally balanced cross-sections (DiPietro and Pogue, 2004; Searle et al., 2007;
286 Gavillot et al., 2018) suggest that the Himalayan wedge is bounded at the base by décollement,
287 named the MHT and all regionally-extensive surface-breaking thrust systems are rooted to it.

288 The orogenic growth of the ~~Himalaya~~Himalaya resulted into an overall in-sequence

289 development of the orogen-scale fault systems which broadly define the morphotectonic sectors
290 of the orogen (Fig. 1b). Notable among those sectors, the Higher Himalaya is bordered by the
291 MCT in the south and is comprised of high-grade metasediments, Higher Himalayan Crystalline
292 Sequence (HHCS) and Ordovician granite intrusives ([Fuchs, 1981](#); [Steck, 2003](#); [DiPietro and](#)
293 [Pogue, 2004](#); [Gavillot et al., 2018](#)). The Low-grade metasediments (quartzites, phyllites, schists,
294 slates) of the Proterozoic Lesser Himalayan sequence are exposed between the MCT in the north
295 and MBT in the south. The Lesser Himalayan domain is narrow (4-15 km) in the NW Himalaya
296 except where it is exposed in the form of tectonic windows (Kishtwar window, Kullu-Rampur
297 window etc.) in the western Himalaya (Steck, 2003). The Sub-Himalayan fold-and-thrust belt
298 lying to the south of the MBT is tectonically the most active sector since the late Quaternary
299 (~~Thakur et al.~~[Gavillot, 2014](#); [Vassallo et al., 2015](#); [Gavillot et al., 2018](#)).

300 Near the southwest corner of our study area, Proterozoic low-grade Lesser Himalayan
301 metasediments are thrust over the Tertiary Sub-Himalayan sediments along the MBT (Wadia,
302 1934; Thakur, 1992). Near the Chenab region [in the Kashmir Himalaya](#), Apatite U-Th/He ages
303 suggest that cooling and exhumation related to faulting along the MBT thrust sheet initiated
304 before $\sim 5 \pm 3$ Myr (~~Kumar et al., 1995~~[Gavillot et al., 2018](#)). Geomorphic data obtained across
305 the MBT in Kashmir Himalaya suggest that MBT has not been reactivated for the last 14-17 kyr
306 (Vassallo et al., 2015). In the [NW-Kashmir](#) Himalaya, the Lesser Himalayan sequence (LHS)
307 exposed between the MBT and the MCT is characterized by a < 10 km-wide zone of sheared
308 schists, slates, quartzites, phyllites and Proterozoic intrusive granite bodies (Bhatia and Bhatia,
309 1973; Thakur, 1992; Steck, 2003). The LHS is bounded by the MCT shear zone in the hanging
310 wall. The MCT hanging wall forms highly deformed nappe exposing lower and higher
311 Haimantas, which are related to the Higher Himalayan Crystalline Sequence (HHCS) (Bhatia

312 and Bhatia, 1973; Thakur, 1992; Yin and Harrison, 2000; Searle et al., 2007; Gavillot et al.,
313 2018). Nearly 40 km NE of the frontal MCT shear zone, MCT fault zone is re-exposed as a
314 klippe in the vicinity of KW is called the Kishtwar Thrust (KT) (Ul Haq et al., 2019) (fig. 1).
315 Within the KW, Lesser Himalayan ~~Rampur~~ quartzites, low-grade mica schists and phyllites
316 along with the granite intrusives are exposed (Fuchs, 1975; Steck, 2003; DiPietro and Pogue,
317 2004; Yin, 2006; Gavillot et al., 2018). ~~(Fig. 2a). KW exposes a stack of LHS nappes in the~~
318 ~~footwall of the MCT (in this case, KT) which is related to the Lesser Himalayan Duplex (LHD),~~
319 ~~characteristic of the central Himalaya (Decelles et al., 2001). Regionally balanced cross-sections~~
320 ~~(DiPietro and Pogue, 2004; Searle et al., 2007; Gavillot et al., 2018) suggest that the Himalayan~~
321 ~~wedge is bounded at the base by décollement, named the MHT.~~

322 2.1. Structural architecture of the LH duplex

323 The sub-surface structural formation beneath the KW is not well-constrained. A recent
324 study by Gavillot et al., (2018) proposes that the KW exposes a stack of LHS nappes in form of
325 the commonly-known Lesser Himalayan Duplex (LH duplex), characteristic of the central
326 Himalaya (Decelles et al., 2001). They also propose the existence of two mid-crustal ramps
327 ~~segments~~ beneath the KW, viz., MCR-1 and MCR-2 (fig. 1b). Based on thermochronological
328 constraints from Kumar et al., (1995), Gavillot et al. (2018) ~~and Kumar et al., (1995)~~, proposed
329 that the core of the window is exhumed with rates 3.2-3.6 mm/yr during the Quaternary, at a
330 higher rate when compared to the surroundings (~0.2-0.4 mm/yr). However, earlier studies by
331 Fuchs (1975) and Frank et al., (1995) provide different insights to the formation of the KW.
332 Fuchs (1975) proposed the existence of two nappes- a. the Chail Nappe and b. the Lower
333 Crystalline Nappe. The Lower Crystalline nappe is partially or completely included in the MCT
334 (KT) shear zone and the Chail nappe encompasses the core of the window (Stephenson et al.,

2000). According to these studies, the Chail nappe has been internally deformed by crustal buckling, tight isoclinal folding causing repetition and thickening of the LH crust.

The Higher Himalayan sequence dips steeply away from the duplex (~65° towards west) (Fig.1, 2a). The frontal horses of the LH duplex expose internally-folded greenschist facies rocks. Although at the western margin of the duplex, the quartzites stand sub-vertically (Fig.1b2c), the general dip amount reduces as we move from west to east for the next ~10-15 km up to the core of the KW. Near the core of the KW, we observed highly-deformed (folded and multiply-fractured) quartzite at the core of the KW (Fig.2d, 2e). We also observed deformed quartz veins of at least two generations, as well as macroscopic white mica. Here, the Chenab River is also very steep and narrow; the rock units are also steeply-dipping towards the east (~55-65°) and are nearly isoclinal and strongly deformed at places (Fig.2f). Towards the eastern edge of the window, however, the quartzites dip much gently towards the east (~20-30°) (Fig.1b), and much lesser folding and faulting have been recognized in the field (Fig.2g).

2.2. Valley morphology

The broad, 'U-shaped' valley profile near the town of Padder at the eastern margin of the KW is in contrast with the interior of the window (Fig.3a). At the core of the KW, the Chenab River maintains a narrow channel width and a steep gradient (Fig.3b). The E-W traverse of the Chenab River through the KW is devoid of any significant sediment storage. However, along the N-S traverse parallel to the western margin of the KW, beneath the Kishtwar surface, ~150-170m thick sedimentary deposits are transiently-stored over the steeply-dipping Higher Himalayan bedrock (Fig.3c). The height of the Kishtwar surface from the Chenab River is ~450m, which means ~280m of bedrock incision by the River since the formation of the Kishtwar surface. Along the N-S traverse of the River, epigenetic gorges are formed as a result of the damming of

358 paleo-channel by the hillslope debris flow, followed by the establishment of a newer channel
359 path (Ouimet et al., 2008; Kothyari and Juyal, 2013). One example of such epigenetic gorge
360 formation near the town of Drabshalla is shown in Fig.3d. Downstream from the town of
361 Drabshalla, the River maintains narrow channel width (< 25 m) and flows through a gorge
362 having sub-vertical valley-walls (Fig.3e). The tributaries originating from the Higher Himalayan
363 domain form one major knickpoint close to the confluence with the trunk stream (Fig.3f). We
364 have identified at least three strath surface levels above the present-day river channel, viz., T1
365 (280 ± 5 m), T2 (170-175 m) and T3 ($\sim 120 \pm 5$ m), respectively (Fig.3g). The first study on
366 sediment aggradation in the middle Chenab valley (transect from Kishtwar to Doda town) was
367 published by Norin (1926). He argued the sediment aggradation in and around the Kishtwar town
368 is largely contributed by fluvioglacial sediments and the U-shaped valley morphology is a
369 marker of past glacial occupancy. In general, we agree with the findings of Norin (1926) and UI
370 Haq et al., (2019) as we observe ~ 100 m thick late Pleistocene fluvioglacial sediment cover
371 unconformably overlying the Higher Himalayan bedrock, most likely to be paleo-strath surface
372 (Fig.4b). At the same time, we do not agree with the interpretation of surface-breaking faults
373 near Kishtwar town by UI Haq et al. (2019). We inspected the proposed fault locations in detail
374 and didn't observe any evidence of large-scale fault movement, including offset, broken and
375 rotated clasts, fault gouges etc. on the proposed fault planes. There is only one evidence of a
376 deformed sand layer which shows tilting and offset (< 1 m). Therefore, we may conclude that we
377 found no strong evidence of any large-scale surface-breaking faults. The fluvioglacial sediments
378 included alternate layers of pebble conglomerate and coarse-medium sand (Fig.4c). The pebbles
379 are moderately rounded and polished suggesting significant fluvial transport. Our field
380 observations suggest that the fluvioglacial sediments have been succeeded by a significant

381 volume of hillslope debris flow and paleo-landslide deposit (Fig.4c). The thickness of the debris-
382 flow deposits is variable. The hillslope debris units and landslide deposits contain mostly
383 massive, highly-angular, poorly-sorted quartzite clasts from the steep western margin of the KW.
384 The hillslope debris units also contain a few fine-grain sediment layers trapped in between two
385 coarse-grained debris layers (Fig.4e). The town of Kishtwar is situated on this debris flow
386 deposit.

387

388 **3. Methods of morphometric analysis and field data collection**

389

390 **3.1.Morphometry**

391 For conducting the morphometric analysis, we have used 12.5m ALOS-PALSAR DEM
392 data (high resolution terrain-corrected) (Fig.5a). This DEM data has lesser issues with artifacts
393 and noises than 30m SRTM data, which fails to capture the drainage network properly in areas
394 populated by narrow channel gorges. Topographic relief has been calculated using a 4km moving
395 window (Fig.5b) and the rainfall distribution pattern has been adapted from 12-year averaged
396 annual rainfall data (TRMM data: Bookhagen and Burbank, 2006) (Fig.5c).

397 **3.1.1. Drainage network extraction**

398 The drainage network and the longitudinal stream profiles were extracted using the
399 Topographic Analysis Kit toolbox (Forte and Whipple, 2019). An equivalent of 10-pixel
400 smoothing of the raw DEM data has been applied to remove noises from the DEM. The
401 longitudinal stream profile of the Chenab trunk stream was processed with the Topotoolbox
402 'Knickpointfinder' tool (Schwanghart and Scherler, 2014). Several jumps/ kinks in the

403 longitudinal profile are seen and those are marked as knickpoints (Fig.6). A 30m tolerance
404 threshold was applied to extract only the major knickpoints.

405 **3.1.2. Basinwide normalized steepness indices**

406 Global observations across a broad spectrum of tectonic and climatic regimes have
407 revealed a power-law scaling between the local river gradient and upstream contributing area:

$$408 \quad S = k_s \cdot A^{-\theta} \quad (1)$$

409 where S is the stream gradient (m/m), k_s is the steepness index ($m^{2\theta}$), A is the upstream
410 drainage area (m^2), and θ is the concavity index (Flint, 1974; Whipple and Tucker, 1999).
411 Normalized steepness-index values (k_{sn}) are steepness indices calculated using a reference
412 concavity value (θ_{ref}), which is useful to compare steepness-indices of different river systems
413 (Wobus et al., 2006). We extracted the k_{sn} values in the study area using the ArcGIS and
414 MATLAB-supported Topographic Analysis Toolkit (Forte and Whipple, 2019) following the
415 procedure of Wobus et al. (2006). We performed an automated k_{sn} extraction using a critical area
416 of $10^6 m^2$ for assigning the channel head, a smoothing window of 500 m, a θ_{ref} of 0.45, and an
417 auto- k_{sn} window of 250 m for calculating k_{sn} values. The slope-breaks, known as the knickpoints
418 (sometimes referred to as knickzones if it is manifested by a series of rapids instead of a single
419 sharp break in profile), were allocated by comparing the change of slope along the distance-
420 elevation plot (Fig.6, 7a). Threshold ‘dz’ value (projected stream offset across a knickpoint) for
421 this study is 30m. Basinwide mean k_{sn} values are plotted using a $1000 km^2$ threshold catchment
422 area (Fig. 5d).

423 Identification of the knickpoints/ knickzones and their relationship with the rock-types as
424 well as with existing structures are necessary to understand the causal mechanism of the
425 respective knickpoints/ knickzones. Knickpoints/(zones) can be generated by lithological,

426 tectonic and structural control. Lithological knickpoints are stationary and anchored at the
427 transition from the soft-to-hard substrate. The tectonic knickpoints originate at the active tectonic
428 boundary and migrate upstream with time. Structural variations, such as thrust fault ramp-flat
429 geometry may cause a quasistatic knickpoint at the transition of the flat-to-ramp of the fault. In
430 such cases, the ramp segment is characterized by higher steepness than the flat segment and ~~often~~
431 at times the ramp ~~is~~may be characterized by a sequence of rapids, forming a wide knickzone,
432 instead of a single knickpoint.

433 **3.1.3. Channel Width**

434 Channel width is a parameter of assessment of lateral erosion/incision through bedrocks
435 of equivalent strength (Turowski, 2009). The channel width of the Chenab trunk stream ~~within~~
436 ~~the elevation range of 600 to 2200 m above the MSL from just downstream of the MBT up to the~~
437 ~~eastern margin of the KW~~ -was derived by manual selection and digitization of the channel banks
438 using the Google Earth Digital Globe imagery (<http://www.digitalglobe.com/>) of minimum 3.2 m
439 spatial resolution. We used the shortest distance between the two banks as the channel width. We
440 rejected areas having largely unparallel channel-banks as that would bias the result. We used a
441 50 m step between two consecutive points for channel width determination. Twenty point-
442 averaged channel width data along with elevation of the riverbed is shown in Fig.7b.

443 **3.1.4. Specific stream power (SSP) calculation**

444 Specific stream power has often been used as a proxy of fluvial incision or differential
445 uplift along the channel (Royden and Perron, 2013; Whipple and Tucker, 1999). Areas of higher
446 uplift/incision are characterized by transient increase in the specific stream power. Channel slope
447 and channel width data were used to analyse the corresponding changes in the specific stream

448 power (SSP) from upstream of the gorge area to the gorge reaches (Bagnold, 1966). The SSP (ω)
449 was estimated using the following equation –

$$450 \quad \omega = \gamma \cdot Q \cdot s / w \quad (\text{Eq. 1})$$

451 Where, γ - unit weight of water, Q – water discharge, s – energy slope considered
452 equivalent to the channel slope; w – channel width. SSP data from selected stretches are shown
453 in Table 1.

454

455 **3.2. Field data collection**

456 **3.2.1. Structural data**

457 We measured the strike and dip of the foliations and bedding planes of the Lesser and
458 Higher Himalayan rocks using the Freiberg clinometer compass. At least five measurements are
459 taken at every location and the average of them has been reported in Fig. 8a. Field photos in the
460 Fig.2 support observed variations in the structural styles.

461 **3.2.2. Rock strength data**

462 Recording rock strength data in the field is important to understand the role of variable
463 rock-type and rock-strength in changes in morphology. It provides us important insights on the
464 genesis of knickpoints whether they are lithologically-controlled or not. It also helps to
465 understand the variations in channel steepness across rocks of similar lithological strength. We
466 systematically measured the rock strength of the main geologic units using a hand-held rebound
467 hammer. Repeated measurements (8-10 measurements at each of the 75 locations throughout the
468 study area) were conducted to measure the variability of rock-strength within the main lithologic
469 units (Fig. 3a7e). All the measurements were taken perpendicular to the bedding/ foliation plane,
470 and, no measurements are from wet surfaces or surfaces showing fractures. Each reading was

471 taken at least 0.5m apart from the previous one. To our benefit, most of the road-cut sections had
472 bedrock-exposures. Except restricted locations, e.g., dam-sites and military bases and outposts,
473 we were able to cover rest of the study area. To add to this, data taken from Higher Himalayan
474 intrusives close to the western margin of the KT are positively-biased as it represents readings
475 only from the leucosomatic layers. Our data from individual sites are smaller in number than
476 what is preferred for checking the statistical robustness of Schmidt hammer data (Niedzielski et
477 al., 2009). Therefore, we combined the data from all sites representing similar lithology and
478 portrayed the mean \pm standard deviation for the same. Field data on rock strength measurement
479 has been provided in Supplementary Table C1.

480 **3.3.Luminescence dating of transiently-stored sediments in and around Kishtwar**

481 Luminescence dating of Quaternary sediments is a globally accepted method for
482 constraining the timing of deposition of sediments across different depositional environments,
483 viz., Aeolian (Juyal et al., 2010), fluvial (Olley et al., 1998; Cunningham and Wallinga, 2012)
484 and glacial origin (Owen et al., 2002; Pant et al., 2006). In this study, we used luminescence
485 dating techniques to constrain depositional ages of several fluvioglacial and fluvial sand layers
486 exposed near the western margin of the KW and further downstream. Although there exists a few
487 persistent problems in luminescence dating of the Himalayan sediments (including poor
488 sensitivity of quartz and numerous cases of heterogeneous bleaching of the luminescence signal),
489 studies over the past couple of decades have also provided a good control on Himalayan
490 sedimentary chronology by using luminescence dating with quartz (Optically stimulated
491 luminescence, OSL) and feldspar (Infra-red stimulated luminescence, IRSL).

492 Samples K-07, K-08 and K-09 were collected from the medium-coarse sand beds of
493 fluvioglacial origin and have been dated with IRSL technique (Preusser, 2003). Standard IR-

494 protocol was used because the OSL signal was saturated and postIR-IR was showing instances of
495 heterogeneous bleaching. Samples K-02 and K-11 were taken from the fine sand-silt layers lying
496 above the debris-flow deposits and have been treated for OSL dating using double-SAR (single
497 aliquot regenerative) protocol (Roberts, 2007). Double-SAR protocol was used to surpass the
498 luminescence signal from tiny feldspar inclusions within individual quartz grains. Samples K-16
499 and K-17 taken above the T3 strath level, as well as the sample K-18, taken from above the T1
500 strath level were treated/ measured following the OSL double-SAR protocol. Samples K-01 and
501 K-06 taken above the bedrock strath near the town of Doda were also measured following OSL
502 double-SAR protocol. The aliquots were considered for equivalent dose (ED) estimation only if:
503 (i) recycling ratio was within 1 ± 0.1 , (ii) ED error was less than 20%, (iii) test dose error was less
504 than 10%, and (iv) recuperation was below 5% of the natural. Fading correction of the IRSL
505 samples K-07 and K-09 were done using conventional fading correction method (Huntley and
506 Lamothe, 2001). For samples showing over-dispersion (OD) $\leq 20\%$, central age model (CAM)
507 has been used for estimation of equivalent dose (De) (Bailey and Arnold, 2006) instead of
508 RMM-based De estimation as prescribed by Chauhan and Singhvi, (2011), useful for samples
509 having higher over dispersion (Table 2). For samples K-16 and K-17 having high OD value,
510 minimum age model (MAM) has been used. Details of sample preparation are provided in
511 supplement.

512 The dose rate was estimated using online software DRAC (Durcan et al., 2015) from the data of
513 Uranium (U), Thorium (Th) and Potassium (K) measured using ICP-MS and XRF (Table 1) in
514 IISER Kolkata. The estimation of moisture content was done by using the fractional difference
515 of saturated vs. unsaturated sample weight (Table 1).

516 **4. Results**

517

518 *4.1. Field observations and measurements*

519 The Chenab River has deeply incised the KW (Fig. 3b and 3e). The LHS rock units
520 exposed within the KW are mainly composed of ~~fine-grain Rampur~~ Quartzites and phyllites, with
521 occasional schists in between. (Steck, 2003; Gavillot et al., 2018). The ~~LHD-Lesser Himalaya~~
522 has been suggested to be an asymmetric antiformal stack with a steeper western flank (dip:
523 70°/west) (Fig.2c). The KW is surrounded by rock units related to the Higher Himalayan high-
524 grade metasedimentary sequence, mainly garnet-bearing mica schists and gneisses. Higher
525 Himalayan rocks close to the western edge of the KW form a ~~syncline klippe~~ with a southwest-
526 verging MCT at its' base. The KT, southern structural boundary of the window margin,
527 accommodating the differential exhumation between window internal and surroundings, ~~—and it~~
528 is expressed as highly deformed sub-vertical shear bands.

529 Along the traverse of the Chenab River through the ~~window-KW~~ and further downstream,
530 two prominent stretches ~~of-along the Chenab River~~ ~20 and ~25-30 km length ~~have been~~
531 ~~identified where the channel gradients are high~~ are characterized by steep channel gradient and
532 ~~we observed~~ associated with a large number sequence of rapids (fig. 3b). These steep segments
533 are also characterized by a very narrow channel width (< 30m) (fig. 3b, 3e). The steepened
534 segments define knickzone rather than a single knickpoint. The knickzones K1 in the trunk
535 stream as well as in the tributaries are hosted over bedrock gorges. Although the knickzone K2
536 pass through a series of old landslides (around Kishtwar town), the rapids have all formed in
537 bedrock channel. ~~—and field evidence confirms that none of them (downstream from the eastern~~
538 ~~edge of the KW).~~ Therefore, neither K1 nor K2 are appears to be related to damming by recent
539 landslides or other mass movements. The eastern margin of the KW is characterized by a wide

540 'U-shaped' valley filled with thick sand layers and coarser fluvioglacial sediments (Fig. 3a)
541 where the Chenab River incises through this Late Pleistocene fill at present.

542 The rock strength data taken along the Chenab trunk stream portray large variations (R-
543 value ranging from 28 to 62) across different morphotectonic segments (Fig.7e). Within the KW,
544 Lesser Himalayan phyllites and schists have low R values (30-35); however, the low-strength
545 schists and phyllites are sparsely present and therefore, they are ignored while plotting the
546 regional rock strength values in Fig.7e. The dominant Rampur-Lesser Himalayan quartzites in
547 KW, as well as the granitic intrusives in the eastern part of the KW, shows very high R values of
548 55-62 and 51-56 respectively (Fig. ~~3a~~7e). Compared to the high R values in the KW, the Higher
549 Himalayan rocks near the KT (western margin of the KW) metasediments show low strength (R:
550 35-45) till the point L2 (Fig. 3b). However, near the western margin of the KW, the migmatites
551 of Higher Himalayan domain show high rock strength (R value: 58±3) (Fig.7e). The rock
552 strength increases within the Haimanta Formation (R: ~~45-50~~44±2) further downstream until it
553 reaches the MCT shear zone at the southern boundary of the Main Himalayan orogen. The R-
554 value in the frontal Lesser Himalaya is moderate (R: ~~40-45~~41±2).

555 The Higher Himalayan sequence dips steeply away from the duplex (~65° towards west)
556 (Fig.2a, 8a). The frontal nappes of the Lesser Himalaya expose internally-folded greenschist
557 facies rocks. Although at the western margin of the duplex, the quartzites stand sub-vertically,
558 the general dip amount reduces as we move from west to east for the next ~10-15 km (Fig. ~~4a~~8).
559 Near the core of the KW, we observed deformed quartz veins of at least two generations, as well
560 as macroscopic white mica. Near the core of the window, where the river is also very steep and
561 narrow, the rock units are also steeply-dipping towards the east (~60-65°) and are extremely
562 nearly isoclinal and vigorously deformed at places (Fig.2d, 2e). Towards the eastern edge of the

563 window, however, the quartzites dip much gently towards the east (~25-30°) and much lesser
564 folding and faulting have been recognized in the field.

565 | The E-W traverse of the Chenab ~~river~~River is completely devoid of any sediment
566 | storage. However, along the N-S traverse parallel to the western margin of the KW, ~150-170m
567 | thick sedimentary deposits are transiently-stored over the steeply-dipping Higher Himalayan
568 | bedrock. The first study on sediment aggradation in Middle Chenab valley (transect from
569 | Kishtwar to Doda town) was published by Norin (1926). He argued the sediment aggradation in
570 | and around the Kishtwar town is largely contributed by fluvioglacial sediments and the U-shaped
571 | valley morphology is a marker of past glacial occupancy. We partially agree to the findings of
572 | Norin (1926) and Ul Haq et al., (2019) as we observe >100m thick fluvioglacial sediment cover
573 | unconformably overlying the Higher Himalayan bedrock along the N-S traverse of the Chenab
574 | River. The fluvioglacial sediments included alternate layers of pebble conglomerate and coarse-
575 | medium sand. The pebbles are moderately rounded and polished suggesting significant fluvial
576 | transport. Our field observations suggest that the fluvioglacial sediments have been succeeded by
577 | a significant volume of hillslope debris. The thickness of the debris-flow deposits is variable.
578 | The hillslope debris units contain mostly coarse-grained, highly-angular, poorly-sorted quartzite
579 | clasts from the frontal horses of the Lesser Himalayan Duplex. The town of Kishtwar is situated
580 | on this debris flow deposit (Fig.9). Along the N-S traverse of the Chenab, we have observed at
581 | least two epigenetic gorges lying along the main channel (Fig. 3d). The active channel has
582 | incised the Higher Himalayan bedrock and formed strath surfaces. We have identified at least
583 | three strath surface levels above the present-day river channel, viz., T1 (280±5 m), T2 (170-175
584 | m) and T3 (~120±5 m), respectively (Fig.3g, 10a).

585 **4.2. Results from morphometric analysis**

4.2.1. Steep stream segments and associated knickpoints

The longitudinal stream profile along the Chenab River does not portray a typical adjusted concave-up profile across the Himalaya (Fig. 6). We observe breaks in slope and concavity at least at ~~four-six occasions~~ localities within a ~150 km traverse upstream from the MBT across the KW. These breaks are defined as knickpoints or knickzones depending on their type characteristics. The slope breaks define the upstream reaches of the steep stream segments. The basinwide steepness indices span from ~30- >750 $m^{0.9}$ across the study area (Fig. 5d). We assigned a threshold value of $k_{sn} > 550$ for the steepest watersheds/ stream segments. Along the traverse, the major knickpoints are L1 (~1770m), K1 (~1700m), K2 (~1150m) and L2 (~800m) respectively (Fig.6).

Already Nennowitz et al., (2018) had proposed a high basin-averaged k_{sn} value of > 300 in the KW. Here in this study, we worked with a much-detailed DEM and stream-specific k_{sn} allocation (Fig.7d), as well as a basinwide steepness calculation. Our results corroborate with the earlier findings, but, predicts the zone of interest in greater detail. It is important to note that by setting a higher tolerance level in the ‘knickpointfinder’ tool in Topotoolbox, we have managed to remove the DEM artifacts from consideration (Schwanghart and Scherler, 2014).

4.2.2. Channel width and valley morphology

The channel width of the Chenab ~~river~~ River is on average low (30-60m) within the core of the KW (Fig. 3b, 7b), and the low channel width continues till the Chenab River flows N-S along the western margin of the KW. However, there are a few exceptions; upstream from the knickpoint L1 in the Padder valley (in which the town of Padder is located), the channel widens (width ~80-100m) and the channel gradient is low (Fig. 3a). The second instance of a wider channel is seen upstream from knickpoint K2, where there is a reservoir for the Dul-Hasti dam.

609 Downstream from K2 within the Higher Himalaya, the channel width ranges from 50-70 m.
610 However, towards the lower stretches of the N-S traverse, the width is even lower (16-52m). The
611 river width increases to 100-200m as Chenab River takes a westward path thereafter. The river
612 width increases beyond 300m until it leaves the crystalline rocks in the hanging wall of the MCT
613 and enters the Lesser Himalaya in the hanging wall of the MBT across the Baglihar dam. Within
614 the frontal LH, the channel width is again lowered (50-80 m).

615 **4.2.3. Changes in specific stream power (SSP)**

616 Discharge-normalized SSP data calculated from the upstream stretches and the
617 knickzones, K1 and K2 show major increase in SSP within the steep knickzones. The increase in
618 SSP from upstream to the knickzones K1 and K2 are 4.44 and 5.02 times, respectively (Table 1).
619 Such high increase in SSP is aided by steepening of channel gradient (Fig.7c) and narrowing of
620 channel bed (Fig.7b).

621 **4.3. Luminescence chronology**

622 The results for the luminescence chronology experiment are listed in Table 2. Samples
623 collected from the fluvioglacial sediments overlain by debris flow deposit, namely as, K07, K08
624 and K09 yield IRSL ages of 104.5 ± 5.9 kyr, 114.4 ± 6.3 kyr, and 119.2 ± 6.8 kyr, respectively.
625 Fading corrections done for samples K07 and K09 yield the correction factors (g%) of 0.89 and
626 1.11 respectively. The sample K08 has not been treated for fading correction, but for easier
627 understanding, we have assumed a constant sedimentation rate between the samples K07 and
628 K09 and extrapolated the 'fading-corrected' age for K08. The oldest sample K09 (132 ± 7 kyr)
629 (fading-corrected IRSL age) is succeeded by samples K08 (126 ± 6 kyr) and K07 (113 ± 6 kyr)
630 respectively. The finer fraction of the hillslope debris overlying the fluvio-glacial deposits yield
631 OSL ages of 81.1 ± 4.6 kyr (K02) and 85 ± 5 kyr (K11) (Fig.6). OSL samples taken from sparsely-

632 preserved sediment layers above the T3 strath surface shows heterogeneous bleaching and hence
633 we provide a minimum age of 22.8 ± 2.1 kyr (sample K16) and 20.5 ± 1.0 kyr (sample K17). One
634 sample taken above T1 strath level is saturated and shows a minimum age of 52.1 ± 2.8 kyr
635 (sample K18) (Table 2). OSL samples K01 and K06 taken from sand layers sitting atop the
636 Higher Himalayan bedrock straths near the town of Doda portray depositional ages of 49.8 ± 2.9
637 kyr and 51.6 ± 2.4 kyr, respectively (Table 2).

639 5. Discussions

640
641 Morphometric parameters are widely used as indicators of active tectonics and transient
642 topography (~~Haek, 1973~~; Kirby and Whipple, 2012; Seeber and Gornitz, 1983). Many studies
643 have used morphometry as a proxy for understanding the spatial distribution of active
644 deformation across certain segments of the Himalayan front (Malik and Mohanty, 2007; van der
645 Beek et al., 2016; Nennewitz et al., 2018; Kaushal et al., 2017). More importantly, some studies
646 have integrated morphometric analysis with ~~rigorous~~ chronological constraints to assess the
647 spatial and temporal variability in deformation within the Sub-Himalaya (Lave and Avouac,
648 2000; Thakur et al., 2014; Vassalo et al., 2015; Dey et al., 2016; Srivastava et al., 2018). All
649 these studies have shown that morphometric indicators can also be used for a qualitative estimate
650 of changes in uplift rate or spatial variations of deformation, even in the Sub-Himalayan domain
651 where the rivers are often alluviated due to high sediment load (Malik and Mohanty, 2007).
652 Therefore, using morphometric indices to examine some prospect areas and using their relative
653 difference as a proxy of relative changes in faulting and differential uplift as well as connecting

654 these regions with nearby regions having chronological constraints on short-intermediate
655 timescale deformation, is a potent option, when applied carefully.

656 | The KW exhibits younger Apatite fission-track cooling ages (~2-3 ~~Ma~~Myr) as compared
657 | to the surrounding Higher Himalaya, which have been interpreted as the result of rapid
658 | exhumation of the LH duplex over 10⁶-year timescale (~~Kumar et al., 1995~~Gavillot et al., 2018)
659 | are higher compared to surrounding Higher Himalaya. However, we lack any measurements of
660 | deformation across the KW ~~on~~-over the 10³-10⁵-year timescale. With the existing AFT data and
661 | assuming that no major changes of the deformation regime have taken place since the
662 | Quaternary, we may well use it for calibration of morphometric proxies and interpolate these
663 | estimates to regions, where no thermochronological constraint exists. Thus, we have come up
664 | with a morphometric analysis of the terrain and combined those results with existing chronology
665 | and structural data as a proxy for the spatial distribution of faulting and fault patterns.

666

667 **5.1. Knickpoints and their genesis**

668 | Already Seeber and Gornitz (1983) showed that the Chenab River is characterized by a
669 | zone of steep channel gradient in the vicinity of the KW. Thiede and Ehlers (2013) demonstrated
670 | a strong correlation between steeped longitudinal river profiles and young thermochronological
671 | cooling ages, suggesting recent focused rock uplift and rapid exhumation along many major
672 | rivers draining the southern Himalayan front. Although, it is still an open debate whether uplift
673 | and growth of the LH Duplex are triggered solely by slip over the crustal ramp of the MHT or
674 | additional out-of-sequence surface-breaking faults are augmenting it (~~Avouac et al., 2001;~~
675 | Herman et al., 2010; Elliot et al., 2016; Whipple et ~~at~~al., 2016).

676 The longitudinal profile of the lower Chenab traverse (below ~2000 m above MSL) is
677 punctuated by two prominent stretches of knickpoint zones (Fig.6). Below we will discuss the
678 potential cause of formation of those major knickpoints in the context of detailed field
679 observation, of existing field-collected structural and lithological data, geomorphic features, rock
680 strength and channel width information (Fig.7).

681 ***5.1.1. Lithologically-controlled knickpoints***

682 The Himalayan traverse of the Chenab River is characterized by large variations in
683 substrate lithology and rock strength (Fig.1, Fig.7e). These variations have inflicted their ‘marks’
684 on the river profile. An instance of soft-to-hard substrate transition happens across the knickpoint
685 L1, lying downstream from the Padder valley, at the eastern edge of the KW (Fig.2a). Across L1,
686 the river enters the LH bedrock gorge (R value > 50) after exiting the Padder valley filled with
687 unconsolidated fluvio-glacial sediments (Fig. 3a). A similar soft-to-hard substrate transition is
688 observed upstream from the MCT shear zone. The corresponding knickpoint L2 represents a
689 change in lithological formation from the sheared and deformed Higher Himalayan crystalline (R
690 value ~35-40) to deep-seated Haimantas (R value ~40-50). There is no field evidence, such as
691 fault splays or ramps, in support of L2 to be a structurally-controlled one.

692 ***5.1.2. Tectonically-controlled knickpoints***

693 Compiling previously-published data on regional tectonogeomorphic attributes (Gavillot
694 et al., 2018) with detailed field documentation of structural styles and tectonic features; we ~~have~~
695 ~~deciphered the role of rock uplift and variable structural styles in the interiors of the NW~~
696 ~~Himalaya~~ identified several proxies to constrain spatial variability in rock uplift and faulting
697 across the KW. We have found at least two instances where knickpoints are not related to change
698 in substrate, nor are they artificially altered.

699 The knickzone K1 (~1700 m above MSL) represents the upstream reach of a steepened
700 stream segment of run-length ~18-20 km. The steep segment represents a drop of ~420m of the
701 Chenab River across a run-length of ~15-20 km (Fig.8c). The upstream and downstream side of
702 K1 is characterized by a change in the orientation (dip angle) of the foliation of the LH bedrock
703 (Fig. 2f, 2g, 8). Across K1, the dips of the foliation planes change from ~30° to ~60-65° towards
704 east. K1 also reflects a change in the channel width (Fig. 7b). The steep segment exhibits a
705 narrower channel through the core of the KW. Near the end of the steep segment, we observed
706 intensely-deformed (folded and fractured) LH rocks (Fig.2d, 2e). There can be two main
707 possibilities for such observation – (1) it may be an active out-of-sequence fault or (2) it may be
708 an inactive fault that defines the floor-thrust of any of the numerous duplex nappes. We do not
709 find any conclusive evidence of recent activity along this deformed zone, which passively
710 favours the second possibility. On the contrary, the observed changes in the geomorphic indices
711 along with stretch of the knickzone K1 and observed increase in the bedrock dip angle may well
712 be explained by a ramp on the basal decollement. This explanation is supported by the existence
713 of mid-crustal ramps in the balanced cross-section from Gavillot et al., (2018). However, the
714 structural orientation of the rocks (Fig.8a) differ considerably than the proposed LH duplex in
715 Gavillot et al., (2008) raising questions about the duplex-model. Our field observations are
716 supported by works from Fuchs (1975), Frank et al., (1995) and Stephenson et al., (2000) who
717 argued against duplexing of multiple thrust nappes and favoured internal folding of Chail nappe
718 for the growth of the KW. We explain this as evidence of faulting within the LH duplex and the
719 steep stream segment represents the ramp of the fault or fault zone between two duplex nappes
720 (Fig.4b). Therefore, we cannot clearly comment whether K1 represents a K1 therefore, reflects
721 the transition from flat to ramp of the MHT or is it indeed an active out-of-sequence thrust-ramp.

722 ~~The steep segment represents a drop of ~420m of the Chenab river across a run-length of ~20 km~~
723 ~~(Fig.2b). In addition to this, we may comment that the schists and phyllites within the Lesser~~
724 ~~Himalayan sequence probably act as the basal planes of the thrust nappes.~~

725 On the other hand, the other knickpoint K2 nearly coincides with the exposure of the KT
726 (Fig.6). K2 cannot be a lithologically-controlled knickpoint as it reflects a hard-to-soft substrate
727 transition from LH rocks (R value > 50) to HH rocks (R value < 45). We acknowledge that just
728 across the point K2, there are some strong leucosomatic layers within the migmatites (R: 58±3),
729 but in general, the migmatites are also deformed. The rock strength measurement was not done
730 in the multiply-fractured units as it would show inaccurate values. However, i
731 n the longitudinal
732 profile, K2 does not represent a sharp slope break because the downstream segment runs parallel
733 for ~25-30 km and not perpendicular to the orientation of all major structures of the orogen,
734 including the KT. Therefore, we performed an orthogonal projection of the E-W trending
735 traverses of the Chenab ~~river~~River and ~~tried to~~estimated an orogen-perpendicular drop of the
736 Chenab across K2 (Fig. 8c). The truncated profile across K2 shows a drop of ~230m of the
737 channel across an orogen-perpendicular run-length of ~5 km. The orogen-parallel stretch of the
738 river exhibits narrow channel width (<30-35m) through a moderately hard HH bedrock (R-value:
739 35-45). The tributaries within this stretch form significant knickpoint at the confluence with the
740 trunk stream (Fig.3f). These evidences hint towards a rapid uplift of the HH rocks near the
741 western margin of the KT and are possibly related to the presence of another crustal ramp
742 emerging from the MHT (Fig.8d). Although we didn't find any field evidence of regionally-
743 extensive fault along the N-S traverse of the Chenab River, similar topographic and
morphometric pattern can be caused by an active out-of-sequence fault.

744 Both the knickzones, K1 and K2 portray transiently-high specific stream power values
745 (Table 1). This signifies the fact that the knickzones are undergoing much rapid fluvial incision
746 than the rest of the study area. If we consider the fluvial incision as a proxy of relative uplift
747 (assuming a steady-state), we ~~may well say~~infer that the knickzones define the spatial extent of
748 the areas undergoing differential uplift caused by movement on the fault ramps.

749 **5.1.3. Knickpoint marking epigenetic gorge**

750 Epigenetic gorges are common geomorphic features in the high-mountain landscape
751 (Ouimet et al., 2008). Epigenetic gorges form when channels of a drainage system are buried by
752 sediment aggradation and during subsequent re-incision, a new river channel is incised. The N-S
753 traverse of the Chenab River is largely affected by hillslope sediment flux (paleo-landslides and
754 debris flow) from the steep eastern flank. The knickpoint K3 situated near the village of Janwas,
755 mark one such instance of epigenetic gorge where the paleo-valley has been filled initially by
756 fluvio-glacial sediments and the channel abandonment was caused by landslides and hillslope
757 debris flow prior to~80 ky (Fig.4b, 4c).

758 **5.2. Sediment aggradation in Chenab valley**

759 The Chenab valley records a net sediment aggradation since the onset of the last glacial-
760 interglacial cycle till ~80 kyr. Fluvio-glacial outwash sediments range from ~110-130 kyr,
761 whereas the hillslope debris rangeranges from ~90 to ~80 kyr (Fig-7Table 2). The chronology of
762 the sediments is in agreement with the overall stratigraphic order of the sediments. We observe
763 net fluvial incision and formation of bedrock strath surfaces since ~80 kyr (Fig.7C10).

764 **5.3. Drainage re-organization and strath terrace formation along Chenab River**

765 Hillslope debris flow from the high-relief frontal horses of the Lesser Himalayan Duplex
766 overlies the fluvio-glacial sediments stored beneath the Kishtwar surface. We argue that the

767 | hillslope debris ~~flow~~ are paleo-landslide deposits had which intervened and dammed the paleo-
768 | drainage of the Chenab River, which might have been flowing through an easterly path than now
769 | (Fig.9). The Maru River, coming from the northwestern corner of our study area was also joining
770 | the Chenab River at a different location (Fig.9). Our argument is supported by field observation
771 | of thick silt-clay layer in the proposed paleo-valley of the Maru River (Fig.9a, 9c). OSL sample
772 | (K18) from the silt-clay layer is saturated and hence only provide the minimum age of 52 ± 3 ky.
773 | We suggest that the hillslope sediment flux ~~have ceased~~ dammed the flow of the Chenab River
774 | and also propagated through the aforesaid wind-gap of the Maru River. The decline in the
775 | depositional energy has resulted into reduction of grain-size. Post-hillslope debris flow, the
776 | Chenab River also diverted to a new path. The new path of the Chenab River upstream from the
777 | confluence with the Maru River is defined by a very narrow channel flowing through the Higher
778 | Himalayan bedrock gorge (Fig.7b). Downstream from the confluence, we are able to identify at
779 | least three levels of strath terraces lying at heights of ~ 280 - 290 m (T1), ~ 170 m (T2) and ~ 120 m
780 | (T3), respectively (Fig.3g,10a). Our field observation suggests that the formation of the straths is
781 | at least ~ 52 kyr-old. The luminescence chronology samples in this study belong to the ~ 150 -
782 | 170 m-thick soft sediments that are stored stratigraphically-up from the T1 strath level. Our field
783 | observations and chronological estimates suggest that the renewed path of the Chenab River,
784 | must have been formed post the hillslope debris flow ~ 80 - 90 kyr but before 52 kyr.

785 | **5. 4. Rapid bedrock incision along Chenab River**

786 | Considering the rate of excavation of softer sediments to be at least an order of magnitude
787 | higher than the rate of bedrock incision (Kothyari and Juyal, 2013; Sharma et al., 2016), we
788 | calculated the minimum bedrock incision rate at the western margin of the KW, using the height
789 | of the T1 strath ($\sim 280 \pm 5$ m) and the average age of the sediments from the Hillslope debris flow

790 deposit. It yields a minimum bedrock incision rate of ~3.1-3.5 mm/yr over the last 80-90 kyr.
791 Considering the saturated OSL sample from the paleo-valley, we estimated the maximum
792 bedrock incision since 52 kyr to be 5.1-5.5 mm/yr. Similarly, using the minimum age estimate of
793 the T3 terrace abandonment, we deduce a maximum bedrock incision rate of ~5.7-6.1 mm/yr
794 since ~21 kyr. However, further downstream, away from the KW, the average bedrock incision
795 rate derived from dated strath surfaces (~36±2 m high from the Chenab River) near the town of
796 Doda is 0.7±0.1 mm/yr (sample K01 and K06). We don't have bedrock incision rates from the
797 core and the eastern margin of the KW, as the core is devoid of sediment storage and the eastern
798 margin is filled with fluvio-glacial sediments and the river is incising the fill.

799 ~~Many studies have used dated strath surfaces to quantify rock uplift rates in the~~
800 ~~Himalaya (Wesnousky et al., 1999; Lave and Avouac, 2001; Mukul et al., 2007; Thakur et al.,~~
801 ~~2014). Assuming the channel hypsometry to be constant during the incision period; we may infer~~
802 ~~the minimum uplift rate on the ramp of MHT to be ~3.1-3.5 mm/y. Our minimum uplift rate~~
803 ~~estimate is in agreement with long-term exhumation rates of 3.2-3.6 mm/y deduced from the KW~~
804 ~~(Gavillot et al., 2018). The deduced uplift rate can be translated to shortening rate by using~~
805 ~~simple trigonometric function. Our field findings suggest that the larger ramp on the MHT~~
806 ~~(MCR-1) have an average dip of ~60°. Considering a similar geometry for MCR-2, we obtained~~
807 ~~a minimum shortening rate of 1.8-2.0 mm/y. On the other hand, considering the minimum ages~~
808 ~~of terrace abandonment, we obtained maximum uplift rates ~5.5-6.0 mm/y, which would~~
809 ~~translate into a shortening rate of ~3.2-3.5 mm/y.~~

810 **5.5. Our findings in context with the previously-published data**

811 AFT-cooling ages by Kumar et al., (1995) showcased ~~a rapid exhumation~~ young cooling
812 ages of from the core of the KW and its western margin (AFT ages: ~2-3 Myr) compared to the

813 | surroundings (AFT age: 6-12 Myr). The high exhumation rates proposed by Gavillot et al.,
814 | (2018) are based on using a geothermal gradient of 35-40°C/km in Dodson's equation assuming
815 | a 1-D model (Dodson, 1973). Additional data and thermal modeling are needed across the KW to
816 | constrain the exhumation rates from vertical transect. However, Lateral-lateral similarities of the
817 | regional topography and age patterns along the Sutlej area, Beas and Dhauladhar Range (Thiede
818 | et al., 2017; Thiede et al., 2009; Stübner et al., 2018) have yielded similar exhumation rates in
819 | the range of 2-3 mm/y. Long-term exhumation rates from the NW Himalaya agree well with
820 | findings of Nennewitz et al. (2018) who correlated the young thermochron ages with high
821 | basinwide k_{sn} values suggesting high uplift rates over intermediate to longer timescales.
822 | However, a study from the Sikkim Himalaya by Abrahami et al., (2016) portrays decoupling
823 | between long-term exhumation rates and millennial-scale basinwide denudation rates. That study
824 | highlighted that in high-elevation glaciated catchments the exhumation rates are significantly
825 | lower than millennial-scale denudation rates. Therefore However, in case of the NW Himalaya,
826 | the proposed range of long-term exhumation rates of 3.2-3.6-3 mm/yr mm/y determined by
827 | Gavillot et al., (2018) agree with the regional data pattern. Although the geomorphic implications
828 | on landscape evolution are valid for provide resolution at shorter timescales than the low-T
829 | thermochron studies, ~~we must comment that~~ our field observations and analysis support a
830 | protracted growth uplift of the ~~LH duplex~~ KW. Unless there has been an recent ongoing growth
831 | ~~of the duplex uplift~~, the geomorphic signatures would have been subdued. Young low-T
832 | ~~thermochron-AFT~~ ages (Kumar et al., 1995) had been sampled from the steepened stream
833 | reaches, where the SSP is high (Table 1). Interestingly, exhumation rates steepened stretches is
834 | ~~~ten times more~~ nearly one order of magnitude higher than that of the Higher Himalayan units in

835 | the ~~hanging wall of the duplex klippe~~. Our estimates of SSP also reflect an increase by ~five
836 | times within the steepened stretches.

837 | Deeply-incised channel morphology, steep channel gradients marked by knickpoints at
838 | the upstream reaches in and around the KW could be explained by the presence of at least two
839 | orogen-parallel mid-crustal ramps on the MHT (Fig.8d). Existence of two mid-crustal ramps has
840 | already been shown through sequential balanced cross-sections for the last 10 Myr across the
841 | Kashmir Himalaya (Gavillot et al., 2018). ~~Translation on the MHT can impart differential uplift~~
842 | of the LH duplex across the two mid-crustal ramps as ramps would show higher uplift/
843 | exhumation. ~~However, the internal structural orientation of the LH duplex published by Gavillot~~
844 | et al., (2018) (cf. Fig.8d) differ considerably from our field observations. Here we provide more
845 | detailed information on structural styles across the KW (Fig.8a, 8d). Our field observation
846 | questions the existence of multiple nappes forming a duplex (Gavillot et al., 2018) and rather
847 | favors anticlinal doming of the pervasively-deformed Chail nappe, as suggested by Fuchs (1975).
848 | We observe pronounced deformation at the core of the KW (Fig. 2d, 2e) suggesting that this is
849 | related to active faulting, crustal buckling or internal folding which maintain continuous rock-
850 | uplift forcing the Chenab River to incise and prevail at the base of the steepened stretch of K1
851 | (Fig. 2d, 2e). Gavillot et al., (2018) proposed that translation on a mid-crustal ramp of the MHT
852 | and no surface-faulting is driving the uplift at the core of the KW (Fig.8d). One alternative
853 | explanation is the existence of a crustal fault-ramp emerging from the MHT. ~~The ramp of the~~
854 | fault zone mentioned above that triggers rapid exhumation of the hanging wall. In this case, out-
855 | of-sequence faulting ~~It~~ causes high relief, steep channel gradients and higher basinwide steepness
856 | indices over the ramp (Fig.7). Similar ramps have been proposed on the MBT beneath the
857 | Dhauladhar Range (Thiede et al., 2017) and in the east of the NW Himalaya (Caldwell et al.,

2013; Mahesh et al., 2015; Stübner et al., 2018; Yadav et al., 2019). Similar mid-crustal ramp (MCR-2) has been proposed for the western margin of the KW by Gavillot et al., (2018). We don't have any direct field evidence of regional surface-breaking faults which could be related to K2 knickzone. However, a rapid fluvial incision and transient increase in morphometric parameter values probably justify the existence of either a mid-crustal ramp or an out-of-sequence surface-breaking fault.

Our ~~findings from the Kishtwar region of the NW Himalaya establishes~~findings from the Kishtwar region of the NW Himalaya establish the importance of morphometric parameters in the assessment of intermediate timescales of 10^4 - 10^6 years. We can resolve regional variations in the tectonic ~~imprint on~~uplift and related landscape evolution by analyzing the topography with high-resolution DEM. ~~Earlier studies used to process larger areas, but the resolution of those data and findings is coarse (Nennewitz et al., 2018).~~

Models explaining the spatial distribution of the high uplift zone in the interiors of the Himalaya favor the existence of a mid-crustal ramp, which has variable dimension, geometry, and distance from the mountain front along-strike of the Himalayan orogeny (Robert et al., 2009). Nennewitz et al., (2018) have proposed that the million-year-timescale shortening achieved in the interior of the Himalaya near the Sutlej-Beas area in the eastern Himachal Pradesh is caused by accentuated rock uplift over a ramp at a mid-crustal depth of ~ 8-25 km on the MHT. In contrast, studies from the Dhauladhar Range in the north-western Himalaya hints the presence of deep-seated crustal ramp on the MBT and yielded a shortening rate of 3 ± 0.5 mm/yr across the MBT over the last 8 Myr and absence of mid-crustal ramp (Deeken et al., 2011; Thiede et al., 2017). The work by Gavillot et al. (2018) favors the existence of at least two mid-crustal ramps beneath the KW (Supplementary Fig.B2). Their suggestion is in agreement with

881 very young AFT cooling ages (1-3 Ma) (Kumar et al., 1995) in the window (Fig.1a).Our data
882 further supports the idea of mid-crustal ramps beneath the Higher Himalayan domain across the
883 Kashmir and NW Himalaya (Webb et al., 2011; Gavillot et al., 2018; Nennevitz et al., 2018) and
884 possibly explains why the seismic hypocenters are clustered in the vicinity of the proposed ramp
885 of MHT. The seismicity is linked to the ongoing deformation of the Lesser Himalayan anticlinal
886 stack or duplex. These studies altogether point out the along-strike variation in the location of the
887 rapidly-uplifting crustal ramp with respect to the southern Himalayan front. The crustal ramp in
888 the nearby Kangra recess is located beneath the Dhauladhar Range at the main Himalayan front,
889 whereas, in the Himalayan transects situated towards the east and west of Kangra recess, the
890 ramps are located ~100km inside from the MBT. Topographic relief and basinwide mean ksn
891 distribution (Fig.5) hint towards the existence of a lateral ramp in between the Kangra and the
892 Jammu-Kashmir Himalayan transects. However, at this moment, we have no conclusive data in
893 support of this claim.

894 Detailed structural mapping and morphometric analysis using high-resolution DEM
895 provide important constraints on the spatial extent of deformation. We are able to resolve the
896 high-relief Kishtwar Window and the surroundings into two major steep orogen-parallel belts/
897 zones (Fig. 5e, 8d) - one at the core of the KW could be an active high-angle fault-ramp
898 emerging from the MHT- or a crustal ramp; and the other one, the smaller one lies observed
899 along the western margin of the KW could be another ramp on the MHT or a surface-breaking
900 fault. We suggest that this has two major implications. One, we have evidence for the structural
901 architecture of the MHT is variable along-strike of the entire Himalayan orogen. The MHT may
902 have a single or multiple mid-crustal ramps at places and may have none in some transects.
903 Alternatively, there may active out-of-sequence faulting in the interiors of the Main Himalayan

904 orogen. Secondly, the Kishtwar Window is still growing and therefore could be the potential
905 source of future seismic activity.

906 Although we speculate an out-of-sequence fault model for the growth of the KW, there is
907 an important concern regarding this model. Long-term crustal shortening estimated from low-T
908 thermochron data (Gavillot et al., 2018) and GPS-derived decadal shortening estimates (Stevens
909 and Avouac, 2015) imply steady crustal shortening of ~13±1 mm/yr. Assessment of late
910 Pleistocene-Holocene crustal shortening across the Sub-Himalayan domain of the Kashmir
911 Himalaya (Gavillot, 2014; Vassallo et al., 2015) suggests that the total Himalayan shortening
912 since late Pleistocene may have been accommodated only within the Sub-Himalaya; therefore,
913 there is no need of additional out-of-sequence faulting in the KW. However, this is again an
914 assumption that the cumulative crustal shortening rate is steady across different timescales.

915

916 **6. Conclusions**

917

918 Our field observation and the characteristics of terrain morphology match well with the
919 spatial pattern of previously-published thermochronological data and ~~unanimously~~ indicate that
920 the Kishtwar Window is undergoing active and focused uplift and exhumation at present, during
921 intermediate timescales, and in geological past since at least the late Miocene. By compiling all
922 the results and published records, we favor the following conclusions:

- 923 1. The Chenab River maintains an over-steepened bedrock channel and a low
924 channel width irrespective of lithological variations across the KW and beyond,
925 suggesting ongoing rapid fluvial incision related to active tectonic rock uplift.

- 926 2. Our field observations, morphometric analysis, and rock strength measurements
927 document that at least two of these major knickzones with steep longitudinal
928 gradients on the trunk stream are non-lithologic and ~~rather are likely can be~~
929 related to differential rock uplift ~~of the rock units~~. The incision potential (specific
930 stream power) in the steepened stretches ~4-5 times higher than the surroundings.
- 931 3. The differential uplift can be explained either by slip on the multiple ramps on the
932 MHT and exhumation of the duplex floor-thrust or by a combination of slip on the
933 MHT ramp and active out-of-sequence faulting. As of now, we do not have any
934 evidence for large-scale out-of-sequence faulting.
- 935 4. Luminescence chronology of the transiently-stored sediments along the Chenab
936 River suggests that the valley had been overfilled by sediments of fluvio-glacial
937 origin as well as by hillslope sediment flux. Massive sediment aggradation during
938 ~130-80 ky led to drainage re-organization and bedrock incision leaving behind
939 strath surfaces.
- 940 5. The late Quaternary bedrock incision rates near the western margin of the KW are
941 high 3.1-3.6 mm/y while away from KW, the incision rates are low (< 1 mm/y).
942 We argue that the high fluvial incision rate can potentially be linked to
943 accommodation of crustal shortening either by growth of the duplex or by active
944 out-of-sequence faulting near KT.

945 To summarize, our new study reinforces the importance of detailed field observation, and
946 morphometric analysis in understanding the neotectonic framework of the interiors of the
947 Himalaya. With additional chronological evidence from the transiently-stored sediments, we
948 showcase high rates of bedrock incision in the interior of the western Himalaya, which could

949 potentially be indicative of tectonic control on landscape evolution. However, to solve the debate
950 of ongoing duplex-growth vs. active out-of-sequence faulting, we would require more field data
951 on active structures and chronological constraints on deformation rates across potentially-active
952 structures.

953

954

955 **Acknowledgments**

956 This study is funded by the DST INSPIRE faculty fellowship program by the Department
957 of Science and Technology, India (grant #DST/INSPIRE/04/2017/003278), and IIT Gandhinagar
958 post-doctoral research fund (IP/IITGN/ES/SD/201718-01). Thiede is supported by German
959 Science Foundation (grant # DFG TH 1317-8 and 9). We thank M.K.Jaiswal and M.Rawat for
960 providing the elemental analysis. We thank Shambhu Das, Avi Das, Niklas Schaaf, Akashsingh
961 Rajput and Chamel Singh for their assistance during fieldwork. We also thank Soumyajit
962 Mukherjee, Rahul Kaushal and Shantamoy Guha for scientific inputs and comments on this
963 manuscript. We acknowledge A. Forte, Y. Gavillot and S. Hergarten for their constructive
964 reviews.

965

966 **Appendix**

967 Additional maps, figures on morphometric analysis and luminescence dating are listed in
968 Appendix A. Data of rock strength measurements provided in Table C1. Luminescence sample
969 processing is elaborated in Appendix B.

970 **Code availability**

971 Authors used open-source codes of Topotoolbox and Topographic Analysis Kit Toolbox
972 for this study.

973 **Data availability**

974 Field data are already provided in Appendix 1. Additional data on luminescence dating
975 can be provided on request.

976 **Sample availability**

977 Samples used for luminescence dating are already mostly-destroyed, therefore it is
978 beyond sharing.

979 **Author contribution**

980 S.Dey, the first author, completed the fieldwork, sample processing,
981 measurements and writing of this manuscript. R. Thiede helped in fieldwork, discussion and
982 writing of this manuscript. A. Biswas performed the initial morphometric analysis. N.Chauhan
983 helped in measurement of luminescence signal and assessment of the data. P.Chakravarti
984 performed the channel width calculations and compiled the rock strength measurements. V. Jain
985 helped in discussion and writing of the manuscript.

986 **Competing interests**

987 The authors declare that they have no conflict of interest.

988

989 **References**

990 [Abrahami, R., van der Beek, P., Huyghe, P., Hardwick, E., & Carcaillet, J. \(2016\). Decoupling of](#)
991 [long-term exhumation and short-term erosion rates in the Sikkim Himalaya. Earth and Planetary](#)
992 [Science Letters, 433, 76-88.](#)

- 993 | ~~Ahnert, F. (1970). Functional relationships between denudation, relief, and uplift in large, mid-~~
994 | ~~latitude drainage basins. American Journal of Science, 268(3), 243-263.~~
- 995 | Bagnold, R. A. (1966). An approach to the sediment transport problem from general physics. US
996 | government printing office.
- 997 | Bhatia, T. R., & Bhatia, S. K. (1973). Sedimentology of the slate belt of Ramban-Banihal area,
998 | Kashmir Himalaya. *Himalayan Geology*, 3, 116-134.
- 999 | Bollinger, L., Henry, P., & Avouac, J. P. (2006). Mountain building in the Nepal Himalaya:
1000 | Thermal and kinematic model. *Earth and Planetary Science Letters*, 244(1-2), 58-71.
- 1001 | Bookhagen, B., Fleitmann, D., Nishiizumi, K., Strecker, M. R., & Thiede, R. C. (2006).
1002 | Holocene monsoonal dynamics and fluvial terrace formation in the northwest Himalaya,
1003 | India. *Geology*, 34(7), 601-604.
- 1004 | ~~Brozovic, N., & Burbank, D. W. (2000). Dynamic fluvial systems and gravel progradation in the~~
1005 | ~~Himalayan foreland. GSA Bulletin, 112(3), 394-412.~~
- 1006 | Burbank, D. W., Leland, J., Fielding, E., Anderson, R. S., Brozovic, N., Reid, M. R., & Duncan,
1007 | C. (1996). Bedrock incision, rock uplift and threshold hillslopes in the northwestern
1008 | Himalayas. *Nature*, 379(6565), 505.
- 1009 | Burgess, W. P., Yin, A., Dubey, C. S., Shen, Z. K., & Kelty, T. K. (2012). Holocene shortening
1010 | across the Main Frontal Thrust zone in the eastern Himalaya. *Earth and Planetary Science*
1011 | *Letters*, 357, 152-167.

1012 Caldwell, W. B., Klemperer, S. L., Lawrence, J. F., and Rai, S. S., 2013, Characterizing the Main
1013 Himalayan Thrust in the Garhwal Himalaya, India with receiver function CCP stacking: Earth
1014 and Planetary Science Letters, v. 367, p. 15-27.

1015 [Colleps, C. L., Stockli, D. F., McKenzie, N. R., Webb, A. A. G., & Horton, B. K. \(2019\).
1016 Neogene Kinematic Evolution and Exhumation of the NW India Himalaya: Zircon Geo-and
1017 Thermochronometric Insights From the Fold-Thrust Belt and Foreland Basin. Tectonics, 38\(6\),
1018 2059-2086.](#)

1019 ~~[Cortés Aranda, J., Vassallo, R., Jomard, H., Pousse Beltrán, L., Astudillo, L., Mugnier, J. L.,
1020 Jouanne, F., Malik, M., & Carcaillet, J. \(2018\). Late quaternary out-of-sequence deformation in
1021 the innermost Kangra Reentrant, NW Himalaya of India: Seismic potential appraisal from 10Be
1022 dated fluvial terraces. Journal of Asian Earth Sciences, 158, 140-152.](#)~~

1023 DeCelles, P. G., Robinson, D. M., Quade, J., Ojha, T. P., Garzzone, C. N., Copeland, P., and
1024 Upreti, B. N., 2001, Stratigraphy, structure, and tectonic evolution of the Himalayan fold-thrust
1025 belt in western Nepal: Tectonics, v. 20, no. 4, p. 487-509.

1026 Deeken, A., Thiede, R. C., Sobel, E. R., Hourigan, J. K., & Strecker, M. R. (2011).
1027 Exhumational variability within the Himalaya of northwest India. Earth Planetary Science Letters,
1028 305(1-2), 103–114. <https://doi.org/10.1016/j.epsl.2011.02.045>

1029 Dey, S., Thiede, R. C., Schildgen, T. F., Wittmann, H., Bookhagen, B., Scherler, D., & Strecker,
1030 M. R. (2016). Holocene internal shortening within the northwest Sub-Himalaya: Out-of-
1031 sequence faulting of the Jwalamukhi Thrust, India. Tectonics, 35(11), 2677-2697.

1032 DiPietro, J. A., & Pogue, K. R. (2004). Tectonostratigraphic subdivisions of the Himalaya: A
1033 view from the west. Tectonics, 23(5).

1034 Duvall, A., Kirby, E., & Burbank, D. (2004). Tectonic and lithologic controls on bedrock
1035 channel profiles and processes in coastal California. *Journal of Geophysical Research: Earth*
1036 *Surface*, 109(F3).

1037 Elliott, J. R., Jolivet, R., González, P. J., Avouac, J. P., Hollingsworth, J., Searle, M. P., &
1038 Stevens, V. L. (2016). Himalayan megathrust geometry and relation to topography revealed by
1039 the Gorkha earthquake. *Nature Geoscience*, 9(2), 174.

1040 Eugster, P., Scherler, D., Thiede, R. C., Codilean, A. T., and Strecker, M. R., (2016). Rapid Last
1041 Glacial Maximum deglaciation in the Indian Himalaya coeval with midlatitude glaciers: New
1042 insights from ¹⁰Be-dating of ice-polished bedrock surfaces in the Chandra Valley, NW
1043 Himalaya: *Geophysical Research Letters*, v. 43, no. 4, p. 1589-1597.

1044 Finnegan, N. J., Roe, G., Montgomery, D. R., & Hallet, B. (2005). Controls on the channel width
1045 of rivers: Implications for modeling fluvial incision of bedrock. *Geology*, 33(3), 229-232.

1046 Flint, J. J. (1974). Stream gradient as a function of order, magnitude, and discharge. *Water*
1047 *Resources Research*, 10(5), 969-973.

1048 Forte, A.M. and Whipple, K.X. (2019). The Topographic Analysis Toolkit (TAK) for
1049 Topotoolbox. *Earth Surface Dynamics*, 7, 87-95.

1050 [Frank, W., Grasemann, B., Guntli, P. E. T. E. R., & Miller, C. \(1995\). Geological map of the](#)
1051 [Kishtwar-Chamba-Kulu region \(NW Himalayas, India\). *Jahrbuch der Geologischen*](#)
1052 [Bundesanstalt, 138\(2\), 299-308.](#)

1053 [Fuchs, G. \(1975\). Contributions to the geology of the North-Western Himalayas. *Geologische*](#)
1054 [Bundesanstalt.](#)

1055 [Fuchs, G. \(1981\). Outline of the geology of the Himalaya. Mitt. osterr. geol. Ges, 74\(75\), 101-](#)
1056 [127.](#)

1057 ~~[Gahalaut, V. K., & Kalpna. \(2001\). Himalayan mid-crustal ramp. *Current Science*, 1641-1646.](#)~~

1058 Gavillot, Y. G. (2014). Active tectonics of the Kashmir Himalaya (NW India) and earthquake
1059 potential on folds, out-of-sequence thrusts, and duplexes.

1060 Gavillot, Y., Meigs, A. J., Sousa, F. J., Stockli, D., Yule, D., & Malik, M. (2018). Late Cenozoic
1061 Foreland-to-Hinterland Low-Temperature Exhumation History of the Kashmir
1062 Himalaya. *Tectonics*.

1063 Gavillot, Y., Meigs, A., Yule, Y., Heermance, R., Rittenour, T., Madugo, C., & Malik, M.
1064 (2016). Shortening rate and Holocene surface rupture on the Riasi fault system in the Kashmir
1065 Himalaya: Active thrusting within the Northwest Himalayan orogenic wedge. *Geological Society*
1066 *of America Bulletin*, 128(7-8), 1070–1094. <https://doi.org/10.1130/B31281.1>

1067 Harvey, J. E., Burbank, D. W., & Bookhagen, B. (2015). Along-strike changes in Himalayan
1068 thrust geometry: Topographic and tectonic discontinuities in western Nepal. *Lithosphere*, 7(5),
1069 511-518.

1070 Herman, F., Copeland, P., Avouac, J.P., Bollinger, L., Mahéo, G., Le Fort, P., Rai, S., Foster, D.,
1071 Pêcher, A., Stüwe, K. and Henry, P., 2010. Exhumation, crustal deformation, and thermal
1072 structure of the Nepal Himalaya derived from the inversion of thermochronological and
1073 thermobarometric data and modeling of the topography. *Journal of Geophysical Research: Solid*
1074 *Earth*, 115(B6).

1075 Hirschmiller, J., Grujic, D., Bookhagen, B., Coutand, I., Huyghe, P., Mugnier, J.-L., and Ojha,
1076 T., 2014, What controls the growth of the Himalayan foreland fold-and-thrust belt?: *Geology*, v.
1077 42, no. 3, p. 247-250.

1078 Kaushal, R. K., Singh, V., Mukul, M., & Jain, V. (2017). Identification of deformation
1079 variability and active structures using geomorphic markers in the Nahan salient, NW Himalaya,
1080 India. *Quaternary International*, 462, 194-210.

1081 Kumar, A., Lal, N., Jain, A. K., & Sorkhabi, R. B. (1995). Late Cenozoic–Quaternary thermo-
1082 tectonic history of Higher Himalayan Crystalline (HHC) in Kishtwar–Padar–Zaskar region,
1083 NW Himalaya: Evidence from fission-track ages. *Journal of the Geological Society of India*,
1084 45(4), 375–391.

1085 Kundu, B., Yadav, R. K., Bali, B. S., Chowdhury, S., & Gahalaut, V. K. (2014). Oblique
1086 convergence and slip partitioning in the NW Himalaya: implications from GPS
1087 measurements. *Tectonics*, 33(10), 2013-2024.

1088 Lavé, J., & Avouac, J. P. (2000). Active folding of fluvial terraces across the Siwaliks Hills,
1089 Himalayas of central Nepal. *Journal of Geophysical Research: Solid Earth*, 105(B3), 5735-5770.

1090 Lavé, J., & Avouac, J. P. (2001). Fluvial incision and tectonic uplift across the Himalayas of
1091 central Nepal. *Journal of Geophysical Research: Solid Earth*, 106(B11), 26561-26591.

1092 Mahesh, P., Gupta, S., Saikia, U., and Rai, S. S., 2015, Seismotectonics and crustal stress field in
1093 the Kumaon-Garhwal Himalaya: *Tectonophysics*, v. 655, p. 124-138.

1094 Malik, J. N., & Mohanty, C. (2007). Active tectonic influence on the evolution of drainage and
1095 landscape: geomorphic signatures from frontal and hinterland areas along the Northwestern
1096 Himalaya, India. *Journal of Asian Earth Sciences*, 29(5-6), 604-618.

1097 Miller, J. R. (1991). The influence of bedrock geology on knickpoint development and channel-
1098 bed degradation along downcutting streams in south-central Indiana. *The Journal of*
1099 *Geology*, 99(4), 591-605.

1100 Mitra, G., Bhattacharyya, K., & Mukul, M. (2010). The lesser Himalayan duplex in Sikkim:
1101 implications for variations in Himalayan shortening. *Journal of the Geological Society of*
1102 *India*, 75(1), 289-301.

1103 Montgomery, D. R., & Brandon, M. T. (2002). Topographic controls on erosion rates in
1104 tectonically active mountain ranges. *Earth and Planetary Science Letters*, 201(3-4), 481-489.

1105 Mukherjee S. (2015) A review on out-of-sequence deformation in the Himalaya. In: Mukherjee
1106 S, Carosi R, van der Beek P, Mukherjee BK, Robinson D (Eds) *Tectonics of the*
1107 *Himalaya*. Geological Society, London. Special Publications 412, 67-109.

1108 ~~Mukul, M., Jade, S., Bhattacharyya, A. K., & Bhusan, K. (2010). Crustal shortening in~~
1109 ~~convergent orogens: Insights from global positioning system (GPS) measurements in northeast~~
1110 ~~India. *Journal of the Geological Society of India*, 75(1), 302-312.~~

1111 Nábělek, J., Hetényi, G., Vergne, J., Sapkota, S., Kafle, B., Jiang, M., Su, H., Chen, J., & Huang,
1112 B. S. (2009). Underplating in the Himalaya-Tibet collision zone revealed by the Hi-CLIMB
1113 experiment. *Science*, 325(5946), 1371-1374.

1114 Nadim, F., Kjekstad, O., Peduzzi, P., Herold, C., & Jaedicke, C. (2006). Global landslide and
1115 avalanche hotspots. *Landslides*, 3(2), 159-173.

1116 Nennewitz, M., Thiede, R. C., & Bookhagen, B. (2018). Fault activity, tectonic segmentation,
1117 and deformation pattern of the western Himalaya on Ma timescales inferred from landscape
1118 morphology. *Lithosphere*, 10(5), 632-640.

1119 Ni, J., and M. Barazangi (1984), Seismotectonics of the Himalayan collision zone: Geometry of
1120 the underthrusting Indian plate beneath the Himalaya, *J. Geophys. Res.*, 89, 1147 – 1163.

1121 Paul, H., Priestley, K., Powali, D., Sharma, S., Mitra, S., & Wanchoo, S. (2018). Signatures of the
1122 existence of frontal and lateral ramp structures near the Kishtwar Window of the Jammu and
1123 Kashmir Himalaya: Evidence from microseismicity and source mechanisms. *Geochemistry,*
1124 *Geophysics, Geosystems*, 19(9), 3097-3114.

1125 Phartiyal, B., Sharma, A., Srivastava, P., & Ray, Y. (2009). Chronology of relict lake deposits in
1126 the Spiti River, NW Trans Himalaya: Implications to Late Pleistocene–Holocene climate-
1127 tectonic perturbations. *Geomorphology*, 108(3-4), 264-272.

1128 Powers, P. M., Lillie, R. J., & Yeats, R. S. (1998). Structure and shortening of the Kangra and
1129 Dehra Dun reentrants, sub-Himalaya, India. *Geological Society of America Bulletin*, 110(8),
1130 1010-1027.

1131 Raiverman, V. (1983). Basin geometry, Cenozoic sedimentation and hydrocarbon prospects in
1132 north western Himalaya and Indo-Gangetic plains. *Petroleum Asia Journal: Petroliferous basins*
1133 *of India*, 6(4), 67-92.

1134 Robert, X., Van Der Beek, P., Braun, J., Perry, C., Dubille, M., & Mugnier, J. L. (2009).
1135 Assessing Quaternary reactivation of the Main Central thrust zone (central Nepal Himalaya):
1136 New thermochronologic data and numerical modeling. *Geology*, 37(8), 731-734.

1137 Robinson, D. M., & Martin, A. J. (2014). Reconstructing the Greater Indian margin: A balanced
1138 cross section in central Nepal focusing on the Lesser Himalayan duplex. *Tectonics*, 33(11), 2143-
1139 2168.

1140 Royden, L., & Taylor Perron, J. (2013). Solutions of the stream power equation and application
1141 to the evolution of river longitudinal profiles. *Journal of Geophysical Research: Earth*
1142 *Surface*, 118(2), 497-518.

1143 Scherler, D., Bookhagen, B., Wulf, H., Preusser, F., & Strecker, M. R. (2015). Increased late
1144 Pleistocene erosion rates during fluvial aggradation in the Garhwal Himalaya, northern
1145 India. *Earth and Planetary Science Letters*, 428, 255-266.

1146 Schwanghart, W., & Scherler, D. (2014). TopoToolbox 2—MATLAB-based software for
1147 topographic analysis and modeling in Earth surface sciences. *Earth Surface Dynamics*, 2(1), 1-7.

1148 [Searle, M. P., Stephenson, B., Walker, J., & Walker, C. \(2007\). Restoration of the Western](#)
1149 [Himalaya: implications for metamorphic protoliths, thrust and normal faulting, and channel flow](#)
1150 [models. *Episodes*, 30\(4\), 242.](#)

1151 Seeber, L., & Gornitz, V. (1983). River profiles along the Himalayan arc as indicators of active
1152 tectonics. *Tectonophysics*, 92(4), 335-367.

1153 Snyder, N. P., Whipple, K. X., Tucker, G. E., & Merritts, D. J. (2000). Landscape response to
1154 tectonic forcing: Digital elevation model analysis of stream profiles in the Mendocino triple
1155 junction region, northern California. *Geological Society of America Bulletin*, 112(8), 1250-1263.

1156 Steck, A. (2003). Geology of the NW Indian Himalaya. *Eclogae Geol Helv*, 96, 147-196.

1157 [Stephenson, B. J., Waters, D. J., & Searle, M. P. \(2000\). Inverted metamorphism and the Main](#)
1158 [Central Thrust: field relations and thermobarometric constraints from the Kishtwar Window, NW](#)
1159 [Indian Himalaya. *Journal of Metamorphic Geology*, 18\(5\), 571-590.](#)

1160 Stevens, V. L., & Avouac, J. P. (2015). Interseismic coupling on the main Himalayan
1161 thrust. *Geophysical Research Letters*, 42(14), 5828-5837.

1162 Stübner, K., Grujic, D., Dunkl, I., Thiede, R., & Eugster, P. (2018). Pliocene episodic
1163 exhumation and the significance of the Muniari thrust in the northwestern Himalaya. *Earth and*
1164 *Planetary Science Letters*, 481, 273-283.

1165 Thakur, V. C. (Ed.). (1992). *Geology of western Himalaya (Vol. 19)*. Pergamon Press.

1166 Thakur, V. C., Joshi, M., Sahoo, D., Suresh, N., Jayangondapermal, R., & Singh, A. (2014).
1167 Partitioning of convergence in Northwest Sub-Himalaya: estimation of late Quaternary uplift and
1168 convergence rates across the Kangra reentrant, North India. *International Journal of Earth*
1169 *Sciences*, 103(4), 1037-1056.

1170 Thiede, R., Robert, X., Stübner, K., Dey, S., & Faruhn, J. (2017). Sustained out-of-sequence
1171 shortening along a tectonically active segment of the Main Boundary thrust: The Dhauladhar
1172 Range in the northwestern Himalaya. *Lithosphere*, 9(5), 715-725.

1173 Thiede, R. C., Bookhagen, B., Arrowsmith, J. R., Sobel, E. R., & Strecker, M. R. (2004).
1174 Climatic control on rapid exhumation along the southern Himalayan Front. *Earth and Planetary*
1175 *Science Letters*, 222(3-4), 791–806. <https://doi.org/10.1016/j.epsl.2004.03.015>

1176 Turowski, J. M., Lague, D., and Hovius, N. (2009). Response of bedrock channel width to
1177 tectonic forcing: Insights from a numerical model, theoretical considerations, and comparison
1178 with field data. *Journal of Geophysical Research: Earth Surface*, 114(F3).

1179 Vassallo, R., Mugnier, J. L., Vignon, V., Malik, M. A., Jayangondaperumal, R., Srivastava, P.,
1180 and Carcaillet, J. (2015). Distribution of the late-Quaternary deformation in northwestern
1181 Himalaya. *Earth and Planetary Science Letters*, 411, 241-252.

1182 Wadia, D. N. (1934). The Cambrian-Trias sequence of north-western Kashmir (parts of
1183 Muzaffarabad and Baramula districts). *Records of the Geological Survey of India*, 68(2), 121-
1184 176.

1185 Webb, A. A. G., Yin, A., Harrison, T. M., C  lerier, J., Gehrels, G. E., Manning, C. E., & Grove,
1186 M. (2011). Cenozoic tectonic history of the Himachal Himalaya (northwestern India) and its
1187 constraints on the formation mechanism of the Himalayan orogen. *Geosphere*, 7(4), 1013-1061.

1188 Wesnousky, S. G., Kumar, S., Mohindra, R., & Thakur, V. C. (1999). Uplift and convergence
1189 along the Himalayan Frontal Thrust of India. *Tectonics*, 18(6), 967-976.

1190 Whipple, K. X., & Tucker, G. E. (1999). Dynamics of the stream-power river incision model:
1191 Implications for height limits of mountain ranges, landscape response timescales, and research
1192 needs. *Journal of Geophysical Research: Solid Earth*, 104(B8), 17661-17674.

- 1193 Whipple, K. X., DiBiase, R. A., & Crosby, B. T. (2013). Bedrock rivers. In Treatise on
1194 geomorphology. Elsevier Inc..
- 1195 Wobus, C. W., Hodges, K. V., & Whipple, K. X. (2003). Has focused denudation sustained
1196 active thrusting at the Himalayan topographic front?. *Geology*, 31(10), 861-864.
- 1197 Wobus, C., Heimsath, A., Whipple, K., & Hodges, K. (2005). Active out-of-sequence thrust
1198 faulting in the central Nepalese Himalaya. *Nature*, 434(7036), 1008.
- 1199 Wobus, C., Whipple, K. X., Kirby, E., Snyder, N., Johnson, J., Spyropolou, K., Crosby, B.,
1200 Sheehan, D & Willett, S. D. (2006). Tectonics from topography: Procedures, promise, and
1201 pitfalls. *Special papers-geological society of America*, 398, 55.
- 1202 Yadav, R. K., Gahalaut, V. K., Bansal, A. K., Sati, S., Catherine, J., Gautam, P., Kumar, K., and
1203 Rana, N., 2019, Strong seismic coupling underneath Garhwal–Kumaun region, NW Himalaya,
1204 India: *Earth and Planetary Science Letters*, v. 506, p. 8-14.
- 1205 Yin, A., & Harrison, T. M. (2000). Geologic evolution of the Himalayan-Tibetan orogen. *Annual*
1206 *Review of Earth and Planetary Sciences*, 28(1), 211-280.

1207

1208 **Figure captions**

1209

1210 **Figure 1:** (a) An overview geological map of the western sector of the Indian Himalaya showing
1211 major lithology (modified after Steck, 2003 and Gavillot et al., 2018) and existing structures
1212 (Vassalo et al., 2015; Gavillot et al., 2018). The tectonic Kishtwar Window (KW) is surrounded
1213 by exposure of MCT, locally known as the Kishtwar Thrust (KT), and exposes the Lesser
1214 Himalayan nappes. The Lesser Himalaya forms a west-verging asymmetric anticline. Apatite

1215 fission-track (AFT) ages are adapted from Kumar et al., (1995). (b) A balanced cross-section of
1216 the NW Himalaya showing the general architecture of the Himalayan orogenic wedge (modified
1217 after Gavillot et al., 2018). Note that, beneath the KW, Gavillot et al., (2018) proposed the
1218 existence of at least two crustal ramps (MCR-1 and MCR-2) on the MHT, translation on which
1219 may have resulted in 3.2-3.6 mm/yr Quaternary exhumation rates across the KW.

1220 **Figure 2:** Lithological units and structural orientations observed in the Chenab valley. (a)
1221 Steeply-dipping HHCS units near the western margin of the KW. (b) Highly-deformed
1222 migmatites at the base of the KT. (c) Sub-vertical quartzite slabs of Chail Formation exposed in
1223 the frontal horses of the LH Duplex (or, anticline). (d) Highly-deformed, sub-vertical and
1224 pervasively folded and compressed quartzite layers within the core of the KW, the base of
1225 stacked LH-nappes forming the hanging wall of the proposed surface-breaking fault (Fig. 8d). (e)
1226 A close-up view of the folded quartzite units. (f) Steeply-dipping units of granite which formed
1227 new penetrative foliation outcropping upstream from the fault-zone. (g) Further upstream from
1228 the fault-zone, the bedrocks are gentler in the eastern edge of the KW.

1229 **Figure 3:** Figure 3: Geomorphic features observed along the Chenab River across the KW. (a)
1230 Where the Chenab River enters the KW, the major tributaries coming from the Zansar Range in
1231 the north are characterized by ‘U-shaped’ valley suggesting repeated glacial occupancy during
1232 the Quaternary. The Chenab valley is unusually wide here providing space for transient storage
1233 of glacial outwash sediments. The present-day River re-incises these sedimentary fills.
1234 Photograph was taken near the town of Padder (cf. Fig.1a). (b) At the core of the KW, the
1235 Chenab valley is V-shaped, steep The Chenab River is steep and maintains a narrow channel
1236 width. (c) Highly-elevated fluvial strath surfaces are preserved in the vicinity of the town of
1237 Kishtwar Fluvial incision observed along the N-S traverse of the Chenab River. Photograph was

1238 taken from south of the Kishtwar town. The Kishtwar surface (~400m high from the river) is
1239 underlain by ~150-170m thick sediment cover overlying the tilted Higher Himalayan bedrock.
1240 The River has incised another ~240m bedrock in this section. (d) Epigenetic gorge formed along
1241 the Chenab River in its' N-S traverse through the HHCS. The town of Drabshalla is built on the
1242 hillslope deposits. (e) Chenab River maintained very narrow channel (width: ~20-25 m) through
1243 moderately-strong HHCS rocks, suggesting tectonic imprint on topography. (f) Formation of
1244 knickpoint at the confluence of the tributary with the trunk stream implying rapid fluvial incision
1245 of the trunk stream. (g) Three levels of strath surfaces observed below the Kishtwar surface. The
1246 strath levels are marked as T1 (~280m), T2 (~170m) and T3 (~120m). OSL dating of fluvial
1247 sediments lying above the T3 surface yield a minimum depositional age of $\sim 21.6 \pm 2.6$ ky.

1248 **Figure 4:** (a) Lithological distribution near the western margin of the KW (cf. Fig.8 for
1249 location). Luminescence sample (OSL and IRSL) locations and respective depositional ages (in
1250 kyr) are shown. Every sample except K16 and K17 are taken above strath level T1. K16 and
1251 K17 are taken from above the T3 level. Note that, the ages reported in italics are minimum age
1252 estimates. (b) A field photograph from the village Janwas, south of the town of Kishtwar,
1253 showing the aggraded sediments lying above the Higher Himalayan tilted bedrock units. (c)
1254 IRSL ages (in kyr) from the fluvio-glacial sediments and OSL age (in kyr) from the hillslope
1255 debris units suggest the valley aggradation probably started at the transition of the glacial to
1256 interglacial phase ~120-130 kyr and continued till ~80 kyr ago. (d) A close-up view (red
1257 rectangle in fig.4c) of the tilted fluvio-glacial sediment layers showing alternate conglomerate and
1258 medium-coarse sand layers. (e) A ~3m thick fine sand layer within the hillslope debris yield
1259 depositional age of $\sim 86 \pm 5$ kyr. Photograph was taken near the village Pochal, northwest of the
1260 town of Kishtwar.

1261 **Figure 5:** Regional variations in (a) topography, (b) topographic relief (moving window of ~4
1262 km) (c) TRMM-derived rainfall (after Bookhagen and Burbank, 2006), and (d) Basinwide
1263 Normalized steepness indices (ksn value) of the region shown dashed box in Figure 1a. (e)
1264 Swath profiles (swath window: 50 km) along the line AB (cf. Fig.5a) demonstrate the orogen-
1265 perpendicular variations in elevation, rainfall and ksn value. KW is characterized by high
1266 elevation, high relief and high steepness, but low rainfall.

1267 **Figure 6:** Longitudinal profile of the Chenab River show major changes in channel gradient
1268 associated with knickpoints in the upstream. It illustrates the major changes in the channel
1269 gradient extend over the full length of the KW and strongest changes are located in the core and
1270 not at the margins of the window. We classified knickpoints on the basis of their genesis. The
1271 substrate lithology along the River is shown. Knickpoints caused by glacial occupancy (G1, G2
1272 and G3) are adapted from Eugster et al., (2016), who reconstructed the timing of maximum
1273 glaciation and extent of glacial cover in source region of upper Chenab River basin during the
1274 last glacial maximum. These knickpoints highlight the importance of glacial erosion in the high-
1275 elevation sectors, especially in the northern tributaries of the Chenab River. Further in this study,
1276 we focused on the area marked by red rectangle.

1277 **Figure 7:** Along-river variations in (a) channel-elevation, (b) channel width, (c) channel
1278 gradient, (d) Normalized steepness index, and (e) rock-strength of non-fractured bedrock units
1279 (R-value taken by rebound hammer) till 165 km upstream from the MBT (point X, cf. Fig.1a).
1280 The mean $R\text{-value} \pm \sigma$ for each rock type has been plotted against their spatial extent. We
1281 identified two distinct zones (K1 and K2) of high channel gradient and steepness index, which
1282 maintain low channel width despite the variable rock strength of the substrate. Knickpoint K3
1283 may have been generated by the formation of the epigenetic gorge along the N-S traverse of the

1284 Chenab River (cf. Fig.3c). Knickpoints L1 and L2 mark the transition of a soft-to-hard bedrock
1285 substrate.

1286 **Figure 8:** (a) Detailed structural data from the study area showing structural and lithological
1287 variations (modified after Steck, 2003; Gavillot et al., 2018). (b) and (c) orogen-perpendicular
1288 drop of the Chenab trunk stream across stretch 1 and stretch 2, respectively, showing transient
1289 increase in steepness over the K1 and K2 knickzone. The orthogonal profile projection method
1290 has been used in the case of K2 (cf. fig.7) to identify the width of the steep segment. (d)
1291 Comparison between two deformation models explaining the observed morphometric variations
1292 across the KW – (a) duplex-growth model (adapted from Gavillot et al., 2018) and (b) active out-
1293 of-sequence fault model.

1294 **Figure 9:** A satellite image of the northern Kishtwar town showing the present-day flow-path of
1295 the Chenab River (cf. Fig.8 for location). Hillslope debris originated from the steep western
1296 margin of the KW (only made of massive white quartzites) and was deposited over fluvio-glacial
1297 and glacio-lacustrine sediments and Higher Himalaya schists bedrock exposed below in the
1298 Kishtwar valley. Massive hillslope sediment flux impeded the paleo-drainage system leaving
1299 behind the paleo-valley of the tributary, the Maru River. Our interpretation of the paleo-drainage
1300 is marked in a white dashed line. (a) A view of the Kishtwar surface from the western margin
1301 of the KW showing present-day gorge of the Chenab River and its tributary. The wind-gap
1302 (paleo-valley) of the tributary is visible. (b) Thick clay-silt deposit in the wind-gap suggests
1303 abandonment of river-flow. The OSL sample is saturated and hence only denotes the minimum
1304 age of valley abandonment/ hillslope debris flow. (c) Overview picture of the frontal horses of
1305 the LH duplex and the direction of debris flow towards the Kishtwar town. (d) Angular, poorly-
1306 sorted clasts and boulders were observed at the base of the debris flow unit near the village of

1307 Pochal, north of the Kishtwar town. The white quartzites of LH are exposed in the vicinity of the
1308 Kishtwar Town (see satellite image) – only the eastern valley flank can have collapsed in the
1309 past.

1310 **Figure 10:** (a) A topographic and geomorphic profile across the Chenab valley drawn over the
1311 Kishtwar Town. The valley aggradation by fluvio-glacial and hillslope debris sediments was
1312 succeeded by a fluvial incision which penetrated through the unconsolidated sediments of
1313 thickness ~140-150m and incised Higher Himalayan bedrock by $\sim 280 \pm 5$ m, leaving behind at
1314 least three recognizable strath surfaces with a thin late Pleistocene sediment cover. The three
1315 strath surfaces are at 280 ± 5 m (T1), ~ 170 m (T2), and $\sim 120 \pm 5$ m (T3) heights from the present-
1316 day River. We assume that the present-day bedrock gorge has been carved since the deposition
1317 of the glacio-lacustrine sediment deposits (~ 100 -130 ky) and the hillslope debris (~ 90 -80 ky)
1318 onto former fluvial strath surface of Higher Himalayan Bedrock. The width of the fluvial strath
1319 surface where the Kishtwar Town is located indicates that the river network had been dammed
1320 earlier too. (b) Graphical representation of mean bedrock incision rates since 80 kyr. Age
1321 constraints for T3 are shown in Fig. 4a. Based on relative heights and depositional ages of late
1322 Pleistocene deposits, we propose a minimum and a maximum bedrock incision rate of 3.1-3.5
1323 mm/y and 5.2-5.6 mm/yr, respectively. However, further downstream, the bedrock incision rates
1324 calculated from bedrock straths farther downstream from the KW range 0.7-0.8 mm/yr.

1325 **Table caption:**

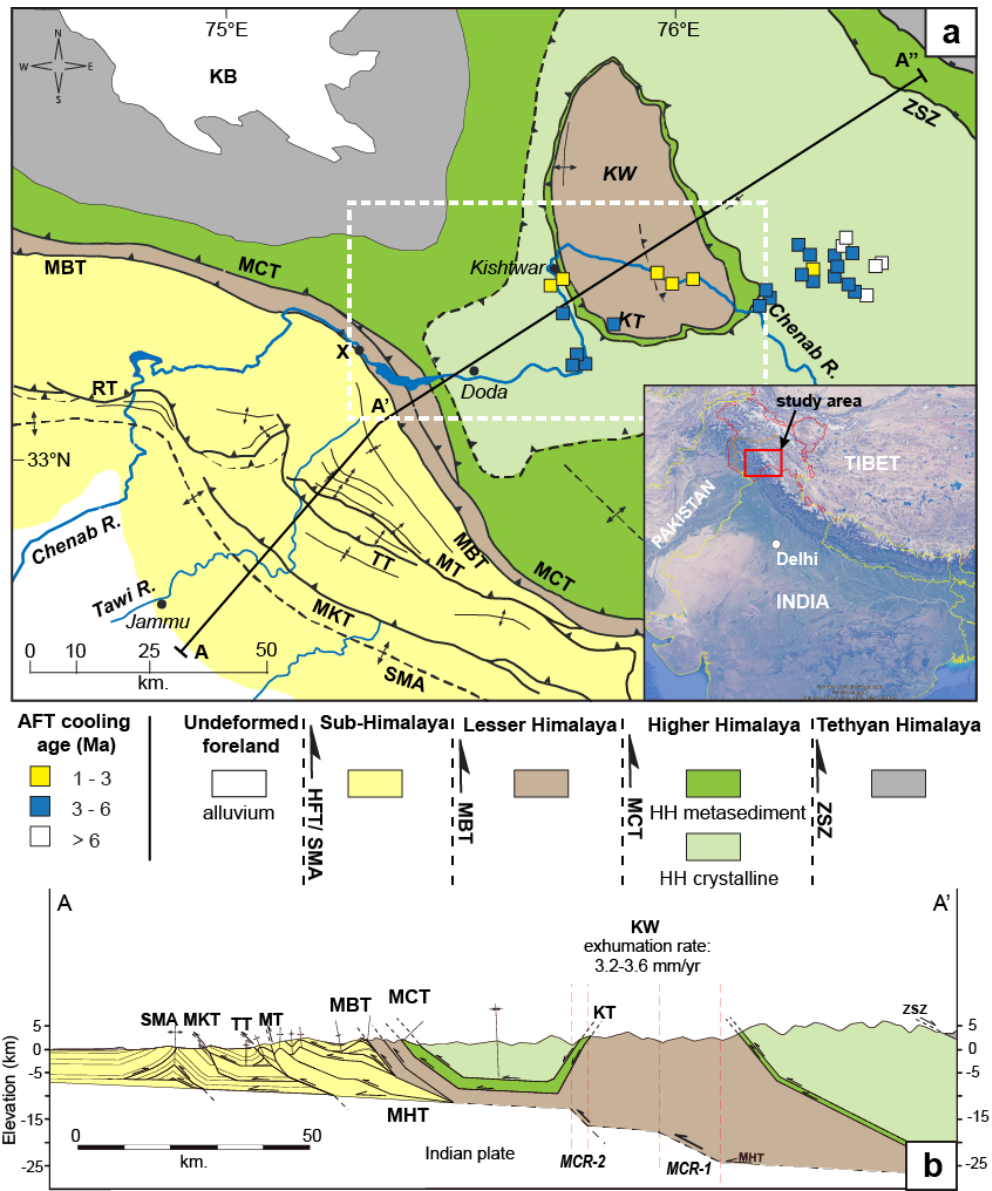
1326 **Table 1:** Calculations of change in specific stream power (SSP) values across the ramp and the
1327 flat segments beneath the LH Duplex. We used a uniform discharge for SSP calculation.

1328 **Table 2:** Sample locations, elemental concentrations, dose rates, equivalent doses and age
1329 estimations for sand samples from Kishtwar valley.

1330 Figures

1331

Figure 1



1332

1333

1334

Figure 2

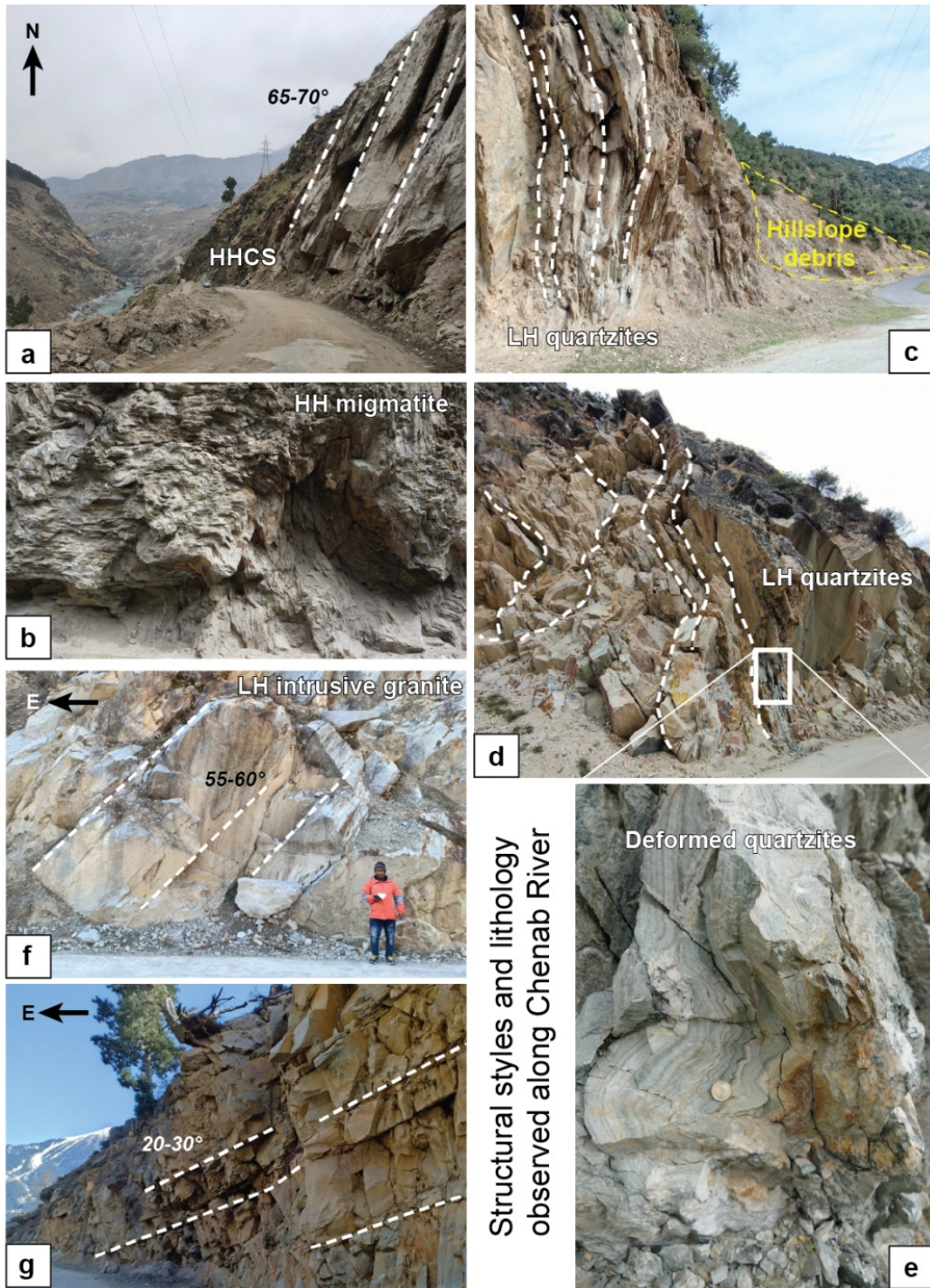


Figure 3

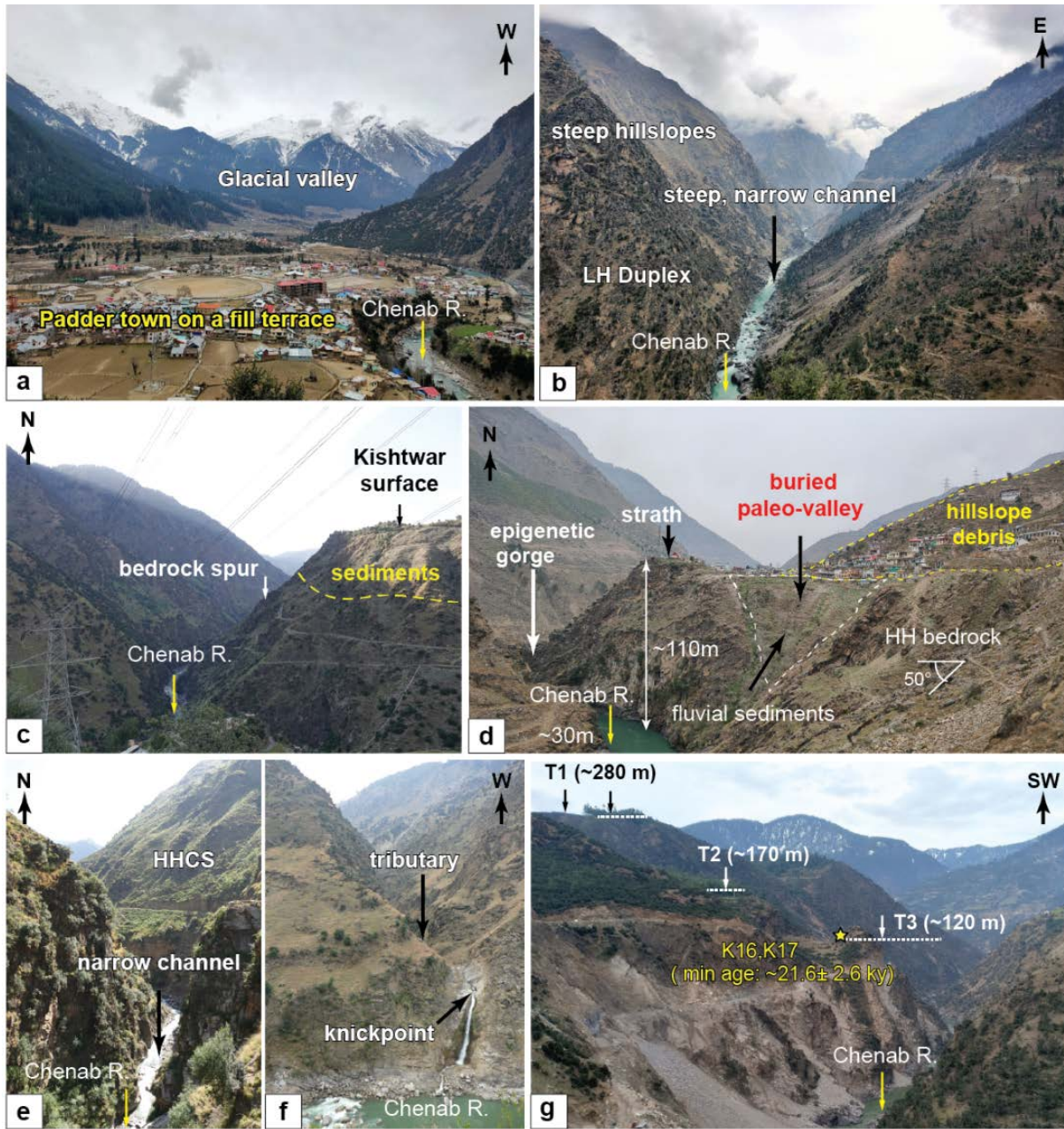
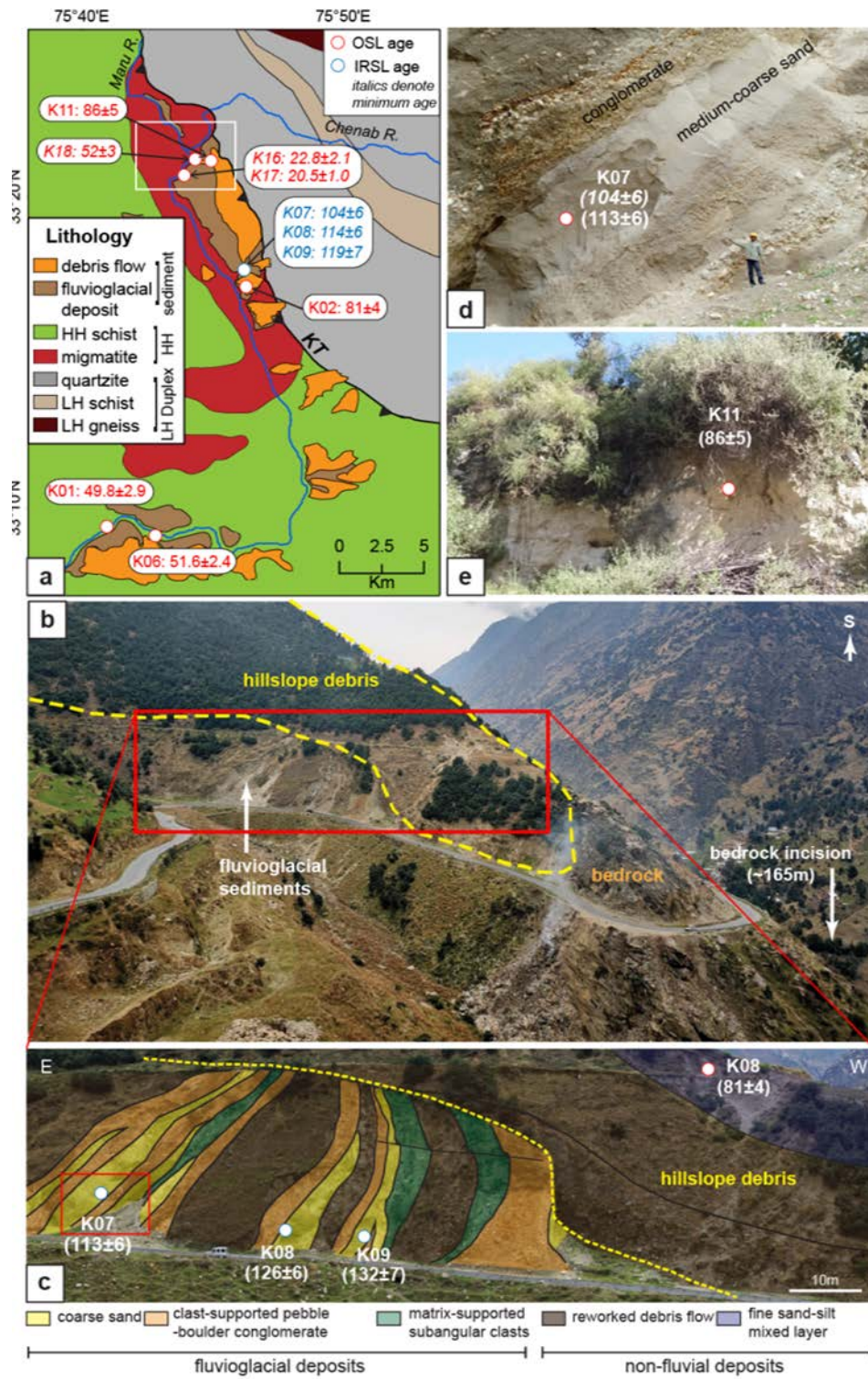
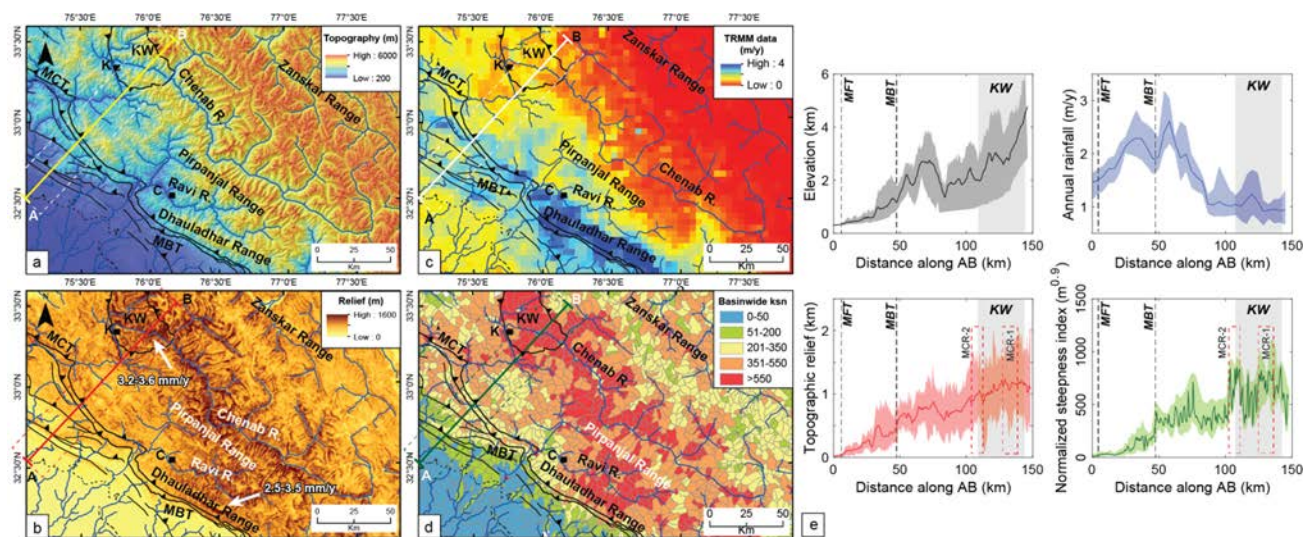


Figure 4



1344

Figure 5

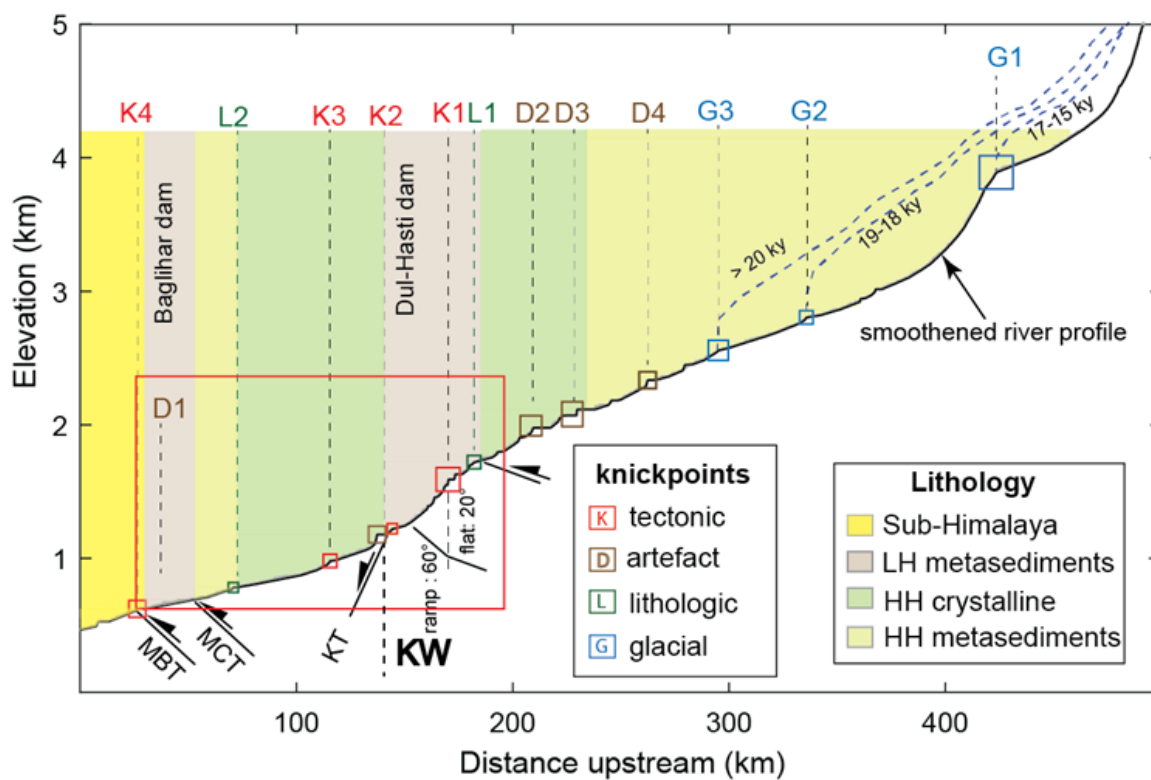


1345

1346

1347

Figure 6



1348

1349

Figure 7

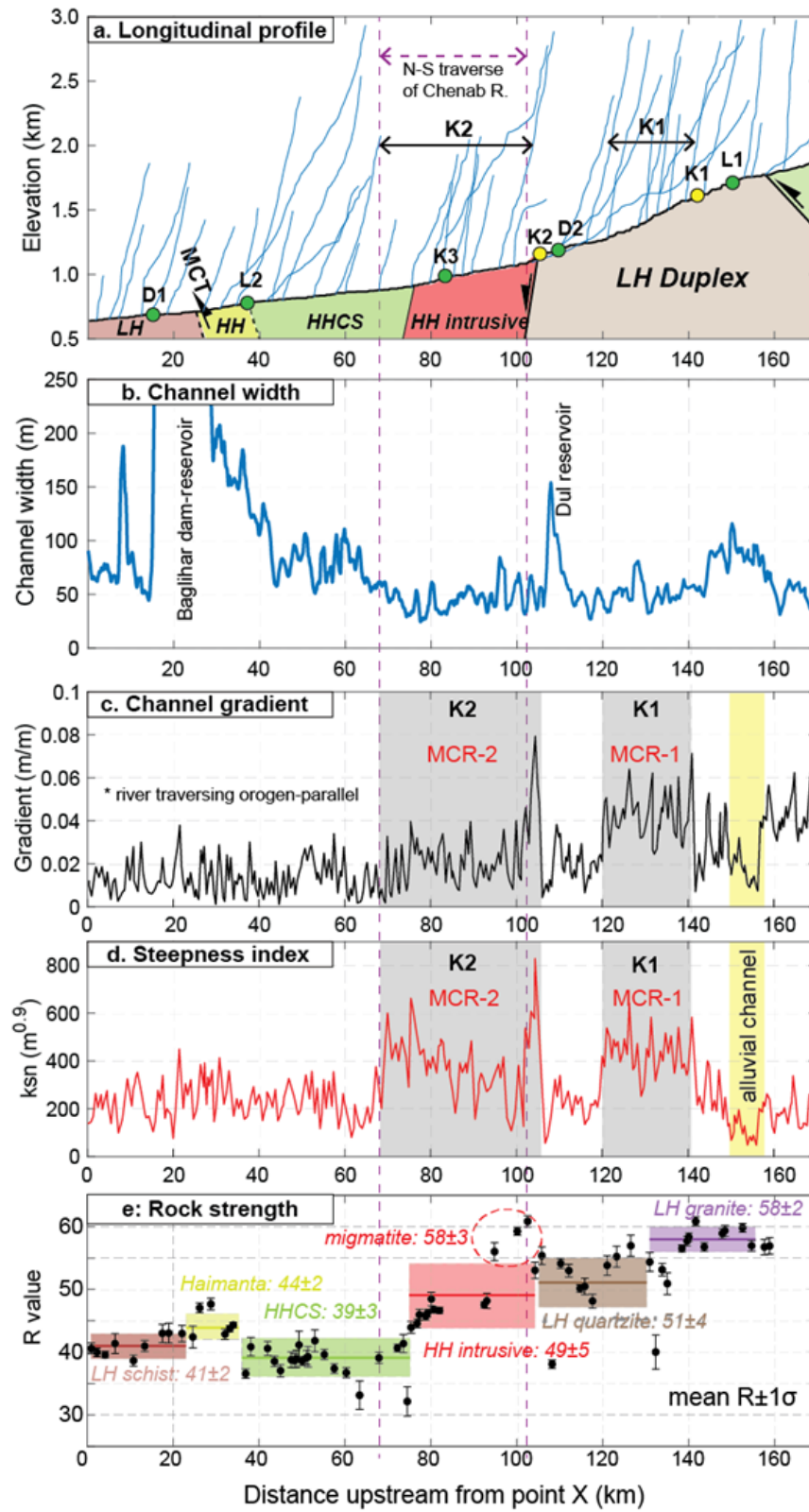
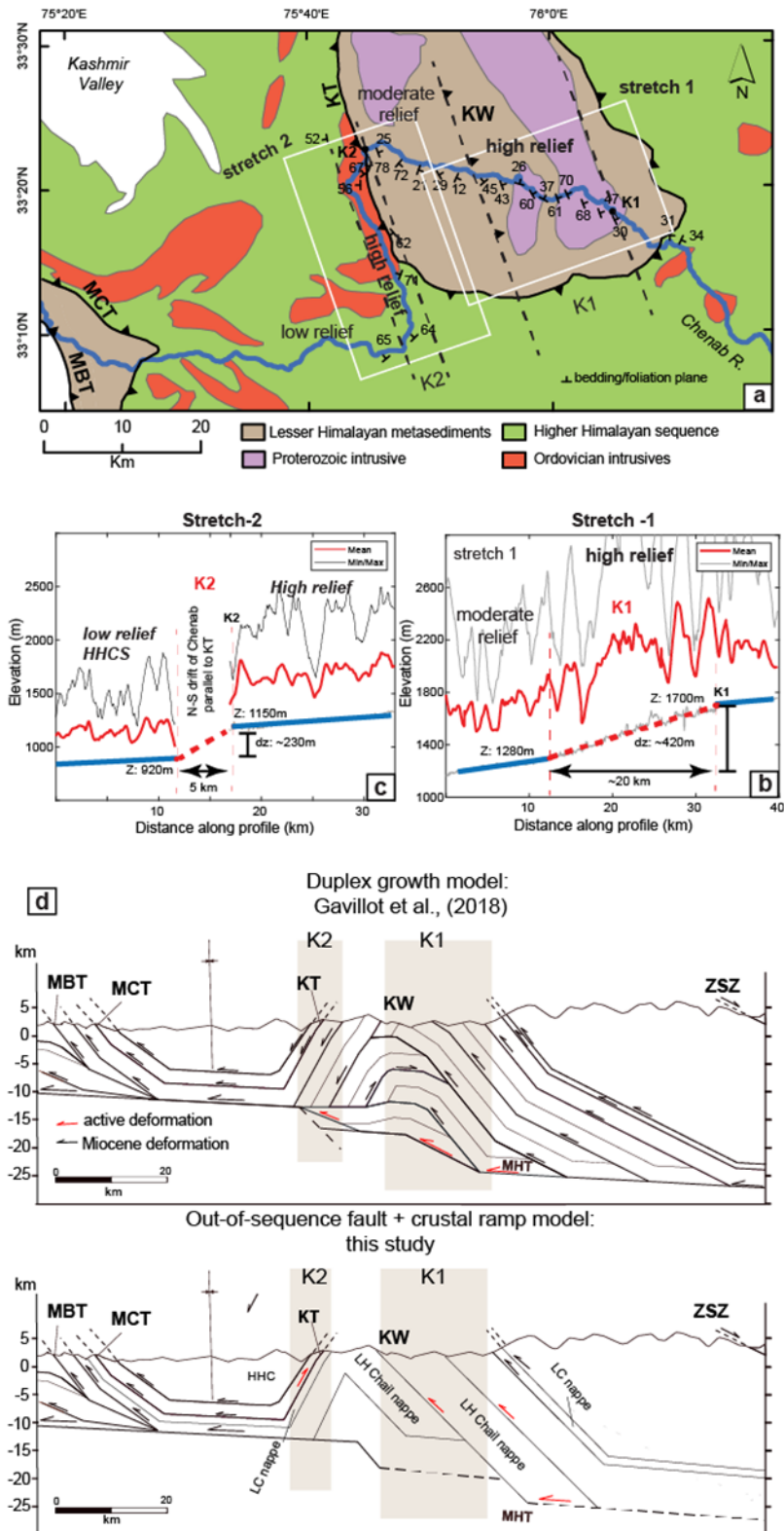
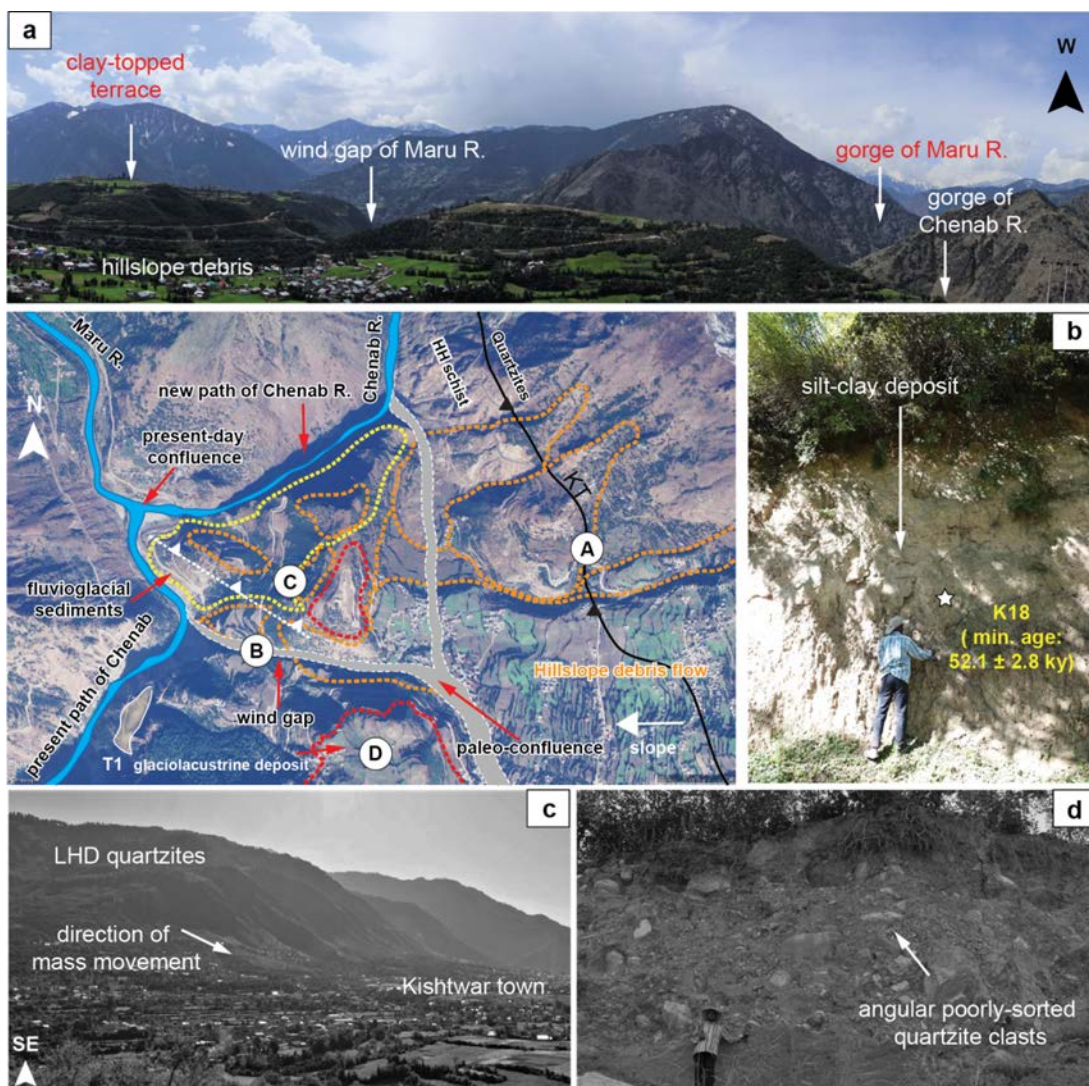


Figure 8



1356

Figure 9

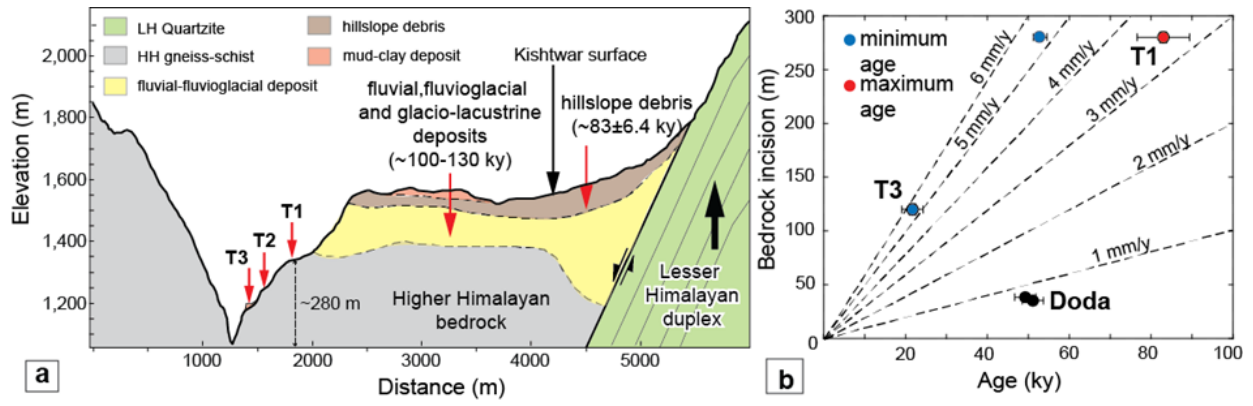


1357

1358

1359

Figure 10



1360

1361

1362

Table 1

Parameter	flat 1	ramp 1	% change	ratio ramp 1:flat 1	flat 2	ramp 2	% change	ratio ramp 2:flat 2
average channel gradient (m/m)	0.006	0.021	250.00	3.5	0.01	0.046	360	4.60
average channel width (m)	70	45	-35.71	0.6	55	42	-24	0.76
*Specific stream power (SSP)	0.000086	0.000467	444.44	5.4	0.000182	0.001095	502	6.02

* SSP calculated by assuming equal-discharge (Q)

1363

1364

1365

Table 2

Sample type	Sample name	Lat (°)	Long (°)	U (ppm)	Th (ppm)	K (%)	water (%)	Dose rate (Gy/ky)	De (Gy)	OD (%)	Age (ky)	fading correction	Corrected age (ky)
using central age model													
OSL	K02	33.29607	75.77619	3.8	7.2	0.46	6.1	1.74±0.02	141±8	19.5	81.1±4.6		
OSL	K11	33.35352	75.74649	3.1	12.7	2.41	6	3.97±0.09	341±19	16.8	85.7±5.1		
OSL	K01	33.15222	75.66323	2.9	13.2	2.03	9	3.88±0.04	193±11	22.1	49.8±2.9		
OSL	K06	33.15243	75.70609	3.4	18.0	2.17	5.4	3.97±0.05	205±10	14.4	51.6±2.4		
IRSL	K07	33.27780	75.76922	3.3	13.8	2.31	5.3	4.67±0.22	489±29	16.8	104.5±5.9	0.89	113±6
IRSL	K08	33.27780	75.76922	3.5	16.9	1.97	5.6	4.61±0.23	528±38	20.5	114.4±6.3		
IRSL	K09	33.27780	75.76922	3.3	12.2	1.98	4.8	4.29±0.20	510±42	18.1	119.2±6.8	1.11	132±7
using minimum age model													
OSL	K16	33.34873	75.73324	3.5	16.8	2.03	7.5	3.95±0.1	90±8	40	22.8±2.1		
OSL	K17	33.34873	75.73324	3.4	18	2.17	10.5	3.96±0.11	81±3.5	46	20.5±1.0		
saturated sample													
OSL	K18	33.35176	75.74325	3.3	18.7	2.61	4.5	4.36±0.13	227±14		52.1±2.8		

1366

1367

1368

1369